TAMPEREEN TEKNILLINEN YLIOPISTO

JARI VÄLIAHO

IMPROVING PERFORMANCE OF A MICROFLUIDIC IMMUNOASSAY USING A FINITE ELEMENT METHOD MODELING

Master of Science Thesis

Examiner: Professor Pasi Kallio,
PhD Lasse Välimaa
Examiners and topic approved in the
Faculty of Science and
Environmental Engineering
meeting on 5.12.2012

TIIVISTELMÄ

TAMPEREEN TEKNILLINEN YLIOPISTO
Biotekniikan koulutusohjelma
VÄLIAHO, JARI: Mikrofluidistisella kasetilla tapahtuvan immunomäärityksen suorituskyvyn parantaminen elementtimenetelmämallinnuksen avulla
Diplomityö, 63 sivua
Marraskuu 2013
Pääaine: Biomittaukset
Tarkastaja: professori Pasi Kallio ja FT Lasse Välimaa (Turun yliopisto)
Avainsanat: Mikrofluidistiikka, europium, nanopartikkeli, immunomääritys, elementtimenetelmämallinnus, vieridiagnostiikka

In vitro-diagnostiikassa eletään murrosvaihdetta. Sen sijaan että näytteitä lähetettäisiin keskuslaboratorioihin analysoitavaksi, pyritään analysointi tekemään yhä enenevissä määrin nopeaan vieridiagnostiikkaan perustuvilla laitteilla suoraan lääkärin toimistossa, sairaalavuoteen vieressä tai jopa potilaan kotona. Nämä laitteet perustuvat yhä enenevissä määrin mikrofluidistiikkaan, jossa pieniä nestemääriä käsitellään mikroskaalan nestekanavissa. Mikrofluidistiikan avulla laitteita on voitu miniatyrisoida, jolloin niiden vaatimia näyte ja reagenssimääriä on saatu pienennettyä merkittävästi. Vierihoitodiagnostiikan osalta määritysten herkkyydet ja havaintorajat eivät kuitenkaan ole vielä perinteisten menetelmien tasolla.

Tämän tutkimuksen tarkoituksena oli selvittää, miten mikrofluidistisen määrityskasetin suorituskykyä voitaisiin parantaa erilaisilla menetelmillä. Tavoitteena oli tarkastella miten eri polystyreenimateriaalit ja geometriat vaikuttavat immunomäärityksen suorituskykyyn.

Tutkimuksessa käytettiin ruiskuvalettuja mikrofluidistiikkakasetteja, joiden pinnalle valmistettiin spesifinen vasta-ainepinta. Analyytin konsentraation havaitsemiseen käytettiin europium-kelaatteja sisältäviä, fluoresoivia nanopartikkeleita, joilla on saatu aikaan suuria signaalitasoja ja parempia herkkyyksiä perinteisiin leimoihin verrattuna. Geometrian osalta immunomäärityksestä luotiin yksinkertaistettu elementtimenetelmämalli (FEM, finite element method), jonka avulla geometrian vaikutuksia pyrittiin tarkasteleman.

Tulokset osoittivat, että epäspesifisen sitoutumisen aiheuttamat taustan signaalitasot ovat lähes samat materiaalista riippumatta, mutta polystyreenilaatu Empera 124N antaa parhaimmat signaalitasot muihin materiaaleihin verrattuna. Alkuperäisten reaktiokammioiden FEM-mallit paljastivat määrityksen voimakkaasti diffuusiorajoitteiseksi. Tämän pohjalta suunniteltiin pienempi reaktiokammio, jossa diffuusiorajoitteisuutta vähennettiin liikuttelemalla näytettä edestakaisin reagoivan pinnan yli määrityksen aikana. Tällä tavalla toteutetun määrityksen herkkyys nousi n. 1.4 kertaisesti ja havaintoraja laski 1mU/L:sta n. 0.52 mU/L:aan. Mikrorakenteiden vaikutusta määritykseen kokeiltiin myös ja niiden käyttäminen reaktiokammiossa nosti herkkyyttä 3.8 kertaisesti.

Tulosten perusteella voidaan todeta että jo yksinkertaisellakin FEM-mallilla voidaan kuvata systeemin toimintaa ja tehdä optimointeja. Pienemmän reaktiokammion ansiosta määrityksen herkkyyttä ja havaintorajaa saatiin parannettua ja samalla pienennettiin myös valmistuksessa käytettävien reagenssien määrää. Edestakaisen virtauksen kontrollointi ja mittauskohdan määritys vaativat vielä parannuksia.

ABSTRACT

TAMPERE UNIVERSITY OF TECHNOLOGY
Master's Degree Programme in Biotechnology
VÄLIAHO, JARI: Improving Performance of a Microfluidic Immunoassay Using a Finite Element Method Modeling
Master of Science Thesis, 63 pages
November 2013
Major: Biomeasurements
Examiner: Professor Pasi Kallio and PhD Lasse Välimaa (University of Turku)
Keywords: Microfluidics, europium, nanoparticle, immunoassay, finite element method modeling, point of care diagnostics

In-vitro diagnostics is currently going through changes. Instead of using central laboratories to analyze samples, point-of-care (POC) diagnostic devices are used more and more. With these devices tests can be performed rapidly near the patient in a doctor's office, at bedside or at a patient's home. Most POC devices are based on microfluidics, where small fluid volumes are handled inside micro scale channels. With microfluidics it has been possible to miniaturize these devices. Thus, their sample and reagent consumption is significantly smaller than in conventional methods. What comes to the performance of POC devices', their sensitivities and limit of detection values are still worse than in conventional methods.

The objective of this research was to study how the performance of a microfluidic immunoassay cartridge would be enhanced. The aim was to study how different polystyrene grades and reaction chamber geometries affect immunoassay performance.

Injection molded microfluidic cartridges were used in the research. Specific antibody coating was fabricated on the reaction chamber surface. Analyte concentration was measured with fluorescence nanoparticles containing europium chelates. These nanoparticles were used as they provide higher signal levels and better sensitivities than conventional fluorescence labels. For studying the effects of geometry, a simplified finite element method (FEM) model was created to simulate the immunoreactions occurring inside a chamber.

Results show that signal levels caused by unspecific binding of labels are similar in all materials, but with Empera 124N polystyrene grade signal levels of specific binding were higher than with other materials. FEM models of original reaction chambers showed that the system is fully diffusion limited. New smaller geometries were designed with the help of the FEM model. The main difference was that sample was moved back and forth over the reaction area during incubation. Measurement sensitivity was increased about 1.4-fold and the limit of detection was decreased from 1 mU/L to 0.52 mU/L. Micro structures on the reacting surface, were also tested and they increased measurement sensitivity by 3.8–fold compared to a smooth surface.

As a conclusion it can be said that already a simple FEM model can be used to describe what happens in a system and how the system can be optimized. As a smaller reaction chamber was used, sensitivity and the limit of detection were enhanced and reagent consumption during fabrication was decreased. There are still some problems concerning the control of reciprocating flow and its repeatability which need to be solved.

PREFACE

This thesis was done at Tampere University of Technology (TUT), in the department of Automation Science and Engineering in 2011-13. Development of a reaction chamber for microfluidic immunoassay cartridge was done as a part of the Ready-to-use Microfluidic Cartridges for Affordable Point-of-care Diagnostics project, shortly ReDia project, funded by TEKES.

I would like to thank my supervisor Professor Pasi Kallio for giving me this opportunity. Especially I would like to thank him for being so patient during the time which it took for me to get this thesis done. I would also like to thank the whole Micro- and nanosystems research group. It has been pleasure to work with you.

In addition I would like to thank Lasse Välimaa from the Department of Biotechnology in University of Turku for giving good advice, providing all the necessary reagents and being the second examiner of the thesis. Also thanks to Jyri Öhrling and others from the Polymer laboratory of TUT for injection molding the cartridges for me, Ville Hautala and Ari Stjerna from the department of Production Engineering in TUT for laser welding the cartridges and Jarkko Mutanen and others from University of Eastern Finland for making laser ablations for the mold.

Special thanks to my family and friends for support during the thesis. Also thanks to Pauliina Mäkilä for proofreading the thesis and supporting me.

Tampere 15th of November, 2013

Jari Väliaho

TABLE OF CONTENTS

ABBREVIATIONS AND NOTATIONS

Abbreviations

Ab	Antibody
Ag	Antigen
Bio-MAb	Biotinylated monoclonal antibody
BP	Binding place
BPD	Binding place density
BSA	Bovine serum albumin
CPS	Counts per second
cTnI	Cardiac troponin I
ELISA	Enzyme linked immunosorbent assay
EOF	Electro-osmotic flow
Eu	Europium
Fab	Antibody binding fragment, part of an antibody which is able to bind on antigen
Fc	Fragment crystallisable part of an antibody
FIA	Fluorescence immunoassay
FEM	Finite element method
HAAA	Human anti-animal antibody
IgG	Immunogloblin G
IVD	In vitro diagnostics
LOD	Limit of detection
NP	Nanoparticle
NPS	Nanoparticle bound on the surface
PDE	Partial differential equation
PMMA	Poly methyl methacrylate
POC	Point-of-care
POCT	Point of care testing
PS	Polystyrene
RIA	Radio isotopic assay
SAv-SH	Thiolated streptavidin
SBC	Styrene butadiene copolymer
TSH	Thyroid stimulating hormone, Thyrotropin
TUT	Tampere University of Technology
UTU	University of Turku

Notations

$\boldsymbol{a}$	Displacement matrix
A	Area of a channel cross-section
Bgr	Average of a background signal
Bgr-σ	Standard deviation of a background signal
$c_{0,i}$	Initial concentration of a compound i
c_i	Concentration of a compound i
c_k	k:th used concentration value
d	Diffusion distance
D_{hyd}	Hydraulic diameter of a channel
D_i	Diffusion coefficient of the compound i
$D_{s,i}$	Surface diffusion coefficient of the compound i
$\boldsymbol{f}$	Matrix for forces balancing loads and initial strains
$\boldsymbol{F}$	Volume force matrix caused by gravity
$\boldsymbol{g}$	Gravity vector
$\boldsymbol{I}$	Identity matrix
k_a	Association rate constant
k_B	Boltzmann's constant, 1.3806488×10^{-23} m^2 kg s^{-2} K^{-1}
k_d	Dissociation rate constant
K_A	Association constant
K_D	Dissociation constant
$\boldsymbol{K}$	Stiffness matrix
L_{entr}	Entrance length
L_i	Plug length of the fluid i
$\boldsymbol{n}$	Boundary normal vector
N	The amount of parallel samples
Nc	The number of different concentrations used in an immunoassay
N_A	The Avogadro constant, 6.022×10^{23} pcs mol^{-1}
$\boldsymbol{N_i}$	Flux vector of the compound i
$\boldsymbol{N}_{s,i}$	Flux vector for surface specie i
p	Pressure
Δp_{cap}	Pressure drop caused by capillary force
$\Delta p_{channel}$	Pressure difference over channel
Δp_{drag}	Pressure drop caused by friction
p_{entr}	Entrance pressure
P	Perimeter of a channel cross-section
v	Average velocity
$\boldsymbol{v}$	Velocity vector
r_{cha}	Radius of a channel
r_i	Stokes-Einstein radius of the compound i
$\boldsymbol{r}$	Matrix for applied loads

R	Reaction rate
R_0	Initial reaction rate
R_{hyd}	Hydraulic resistance
R_i	Reaction rate for the compound i
$R_{b,i}$	Reaction rate occurring between surface and bulk solution (for compound i)
$R_{s,i}$	Reaction rate occurring between surface species (for compound i)
Re	Reynolds number
$\bar{s}_{c_k}$	Signal average of used concentration c_k
s_{0_i}	Signal value from zero sample number i
t	Time in seconds
T	Temperature in kelvins
V_0	Flow rate at the inlet
γ	Surface tension
γ_{LG}	Surface tension between liquid and gas
γ_{SG}	Surface tension between solid and gas
γ_{SL}	Surface tension between solid and liquid
Γ_s	Amount of binding places on the surface
δ_i	Site occupancy number for compound i
θ	Contact angle
θ_A	Contact angle of advancing meniscus
θ_i	Fraction of filled binding places by the compound i
θ_R	Contact angle of receding meniscus
μ	Dynamic viscosity
μ_i	Dynamic viscosity of fluid i
ρ	Fluid density
σ_N	Standard deviation of a noise level
σ_0	Standard deviation of a zero sample
$[Ab]$	Concentration of antibodies
$[Ag]$	Concentration of antigens
$[AbAg]$	Concentration of antibody-antigen complexes
$[BP]$	Surface concentration of binding places
$[NP]$	Concentration of nanoparticles
$[NPS]$	Surface concentration of bound nanoparticles

1 INTRODUCTION

1.1 ReDia project

This thesis is a part of Tekes-funded ReDia project which was started on April 2011. Main objective of the project is to develop ready-to-use microfluidic cartridges for affordable point-of-care diagnostics. The project aims to develop a point-of-care (POC) testing cartridge for tuberculosis and cardiac troponin I (cTnI). The project is performed in co-operation with Tampere University of Technology (TUT), University of Turku (UTU) and University of Delhi. Companies included are DHR Finland/Innotrac Diagnostics, Jatec, Kaivogen, Kaptas, Medisize, Medix Biochemica, NanoFoot and Span diagnostics Ltd. (India). The department of Automation Science and Engineering in TUT acts as a project coordinator and is responsible for microfluidics. The department of Production Engineering in TUT focuses on an assembly of cartridges and has knowledge on laser welding. Department of Biotechnology in UTU has knowledge about nanoparticles and other chemistry on the cartridge. The project is organized into three work packages:

1. Production technologies for affordable microfluidic immunoassays
    1. Channel fabrication using injection molding
    2. Channel bonding using laser welding
    3. Material processing using gamma irradiation
    4. Reagent deposition
    5. Product integration

2. Microfluidic tuberculosis assay
    1. Production of capture and detection antibodies
    2. Engineered monoclonal antibody against antigens of mycobactericum tuberculosis
    3. Setting up a heterogeneous nanoparticle assay for tuberculosis in a microfluidic cartridge
    4. Demonstration of the heterogeneous nanoparticle-based tuberculosis assay
    5. Evaluation of the heterogeneous nanoparticle-based tuberculosis assay using clinical samples

3. Microfluidic cTnI assay
    1. **Design of a reaction chamber for heterogeneous cTnI assay**
    2. Setting up a heterogeneous cTnI assay in a microfluidic cartridge
    3. Development of microfluidic sample pre-processing methods
    4. Demonstration of the heterogeneous nanoparticle-based cTnI assay
    5. Evaluation of the heterogeneous nanoparticle-based cTnI assay using clinical samples
    6. Development of sample introduction methods

This thesis covers mostly part 3.1 where the objective is to improve performance of the assay in the cartridge by testing different geometries, cartridge materials and washing procedures for the reaction chamber. Instead of cTnI, TSH is used as a model assay.

1.2 Microfluidic cartridge for immunoassay

ReDia-project uses a disposable immunoassay cartridge which was first designed in an earlier NanoFlow project (Figure 1.1). The cartridge is designed to perform several microfluidic tasks to ensure a reliable result from an immunoassay:

1. Sample inlet
2. Channel for buffer solution
3. Volume metering
4. Mixer
5. Channel containing dried Eu-nanoparticle labels
6. Reaction chamber containing a dried immunoassay surface
7. Chamber for washing solution
8. Waste chamber

The operational principle of the cartridge is as follows. First, blood or plasma sample is inserted in the cartridge through inlet (1). Pressure difference is used to drive the sample plug to the end of the sample channel where certain volume of sample is metered (3). Then the sample plug is mixed (4) with buffer solution (2). Mixing will dilute analyte and it may cause lower signal levels in fluorescence measurements, but it is needed to avoid a hook effect and to decrease a matrix-effect.

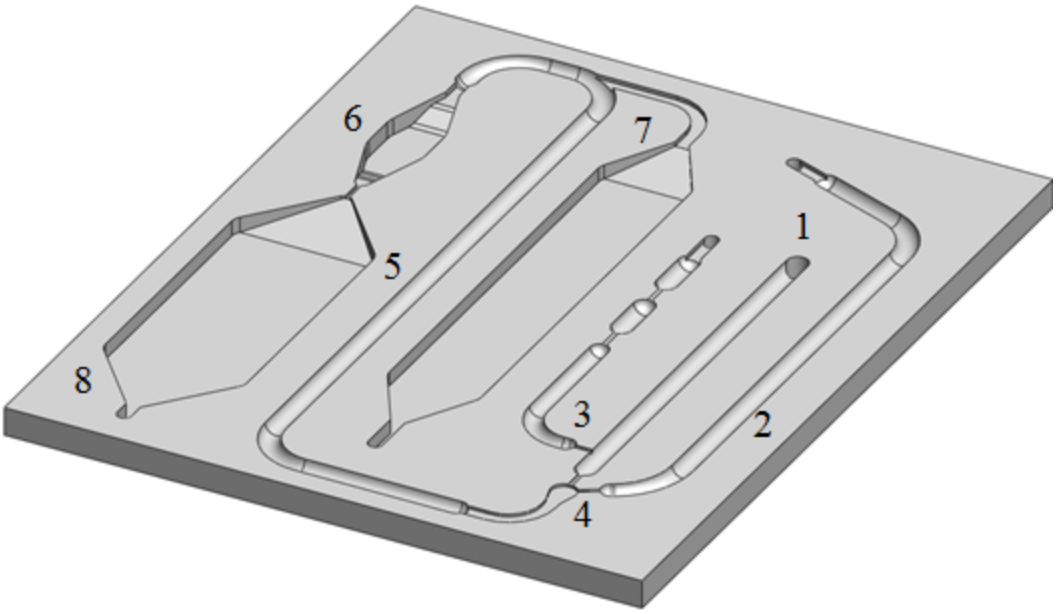

Figure 1.1. *Schematics of the microfluidic immunoassay cartridge at the beginning of the ReDia-project.*

Next comes the immunoassay part: Sample is driven in to the reaction chamber (6) through a channel where Europium nanoparticle labels have been dried (5). Nanoparticles diffuse in the sample and begin to bind analyte on their surface. In the reaction chamber, analyte binds also on the antibodies which are coated on the surface of the reaction chamber. Therefore, nanoparticle labels which have bound analyte will also bind to the surface. Sample is incubated at 37 ℃ for 15 minutes and then the chamber is washed with washing solution. Washing solution is driven from the washing solution chamber (7) to the waste chamber (8). It will remove all unbound particles from the reaction chamber leaving the specifically bound particles on the surface. In the last step fluorescence is measured using a time-resolved fluorometer and the original concentration of the analyte in the sample can be derived from the result.

1.3 Overview of the thesis

In this thesis, the performance of a sandwich immunoassay is studied in microfluidic cartridges. Especially, functionality of the reaction chamber is studied. Earlier studies have shown that there remain problems with unspecific binding of excess nanoparticles in the reaction chamber. This unspecific binding increases the noise in the measurement. Due to the noise, detection of small amounts of analyte is limited.

1.3.1 Goal of the research

The main goal of the study is to enhance the immunoassay performance by increasing sensitivity or decrease limit of detection by studying the effects of material and geometrical designs of the reaction chamber. A finite element method (FEM) model of reactions in the reaction chamber was developed. The purpose of modeling is to provide

a better understanding of what happens inside the chamber. When these phenomena are understood, the model can be used to design a better functional chamber for the cartridge.

1.3.2 The structure of the thesis

The structure of the thesis is following. Chapter 2 includes theory and literature review of the point-of-care (POC) diagnostics, microfluidics, immunoassays and the detection method. The basic principle of finite element method modeling is also presented. Chapter 3 discusses materials and methods used to perform immunoassays. In the same chapter, developed models are described. Chapter 4 presents results and discusses the reasons for the results. Chapter 5 includes final conclusions and future development ideas.

2 LITERATURE REVIEW AND THEORY

This chapter describes literature review and theory part needed in understanding the rest of the thesis. First, the point-of-care concept is introduced to give some background knowledge needed to understand what the thesis is about. The second section introduces the microfluidic concept and its phenomena. The third section explains immunoassay principles and the fourth section introduces interferences these immunoassays may have. The fifth section explains parameters affecting the immunoassay performance. Especially term sensitivity is explained there. In the sixth section, time-resolved fluorescence as a detection method is explained. The seventh section describes shortly the idea of finite element method modeling.

2.1 Point-of-care diagnostics

2.1.1 In vitro diagnostics

In vitro diagnostics (IVD) includes all diagnostics where a sample is taken from a patient and measurements are done outside the patient. Typical samples are bodily fluids like urine, saliva or blood products from where different analytes like hormones, proteins and DNA are measured using different methods. IVD is usually done in centralized laboratories where patient samples are sent from surrounding hospitals.

The revenues in Western Europe IVD market were over $ 13 110 million in 2011 and it is estimated to grow annually by 7.8 % and reaching revenues over $ 22 211 million in 2018. Revenues of point-of-care testing (POCT) were only $ 1 535 million but it is one of the fastest growing segment in IVD market with the estimated annual growth of 8.5 %. [1]

2.1.2 Point-of-care testing

Point-of-care testing is rapid in vitro diagnostics done near the patient. The idea of the POCT is that only small sample volume is needed, measurement can be done in minutes and care can be planned earlier compared to centralized laboratory tests. When adapting POC systems things happen faster. The doctor can get a result during one meeting and decide whether patient needs antibiotics or not. This helps to decrease the use of unnecessary antibiotics and reduces the time a patient stays in a hospital. Thus, developing and adopting rapid and cost-efficient POC tests would significantly improve public health care and decrease total expenses caused by the health care system.

Desired features for point of care diagnostics are (i) small reagent consumption for decreasing manufacturing costs and demanded sample volume to make tests minimally invasive and more convenient for the patient to take. (ii) Turnaround time, time from taking a sample to getting the results, should be less than 20 minutes which means that the test can be done, results can be analysed and future care can be decided during one doctor's office meeting. In centralized IVD tests this is not possible due to sample deliveries and long measuring times. Delivery may also affect sample composition and thus it is possible to measure some analytes only right after taking the sample. [2–4]

Generally centralized IVD gives more (iii) sensitive and (iv) specific results which are more (v) reproducible due to longer reaction times, but POC tests have been developing all the time and it is already more used for abundant analytes, like blood glucose or pregnancy tests. Portability (vi) is a significant benefit of POC devices as testing can be done in different environments like at a doctor's office, at an ambulance, at an emergency site or at home. To be usable by untrained personnel (vii) the device must have a simple user interface, or even better, be as automated as possible. Environmental effects like the temperature or humidity caused by the location may affect performance and thus the device must be robust (viii) against such factors. Portability set also a demand for data transfer (ix) in situations where the user is not able to do an analysis or data is needed by surgeons to prepare a surgery of an incoming emergency patient. Data transfer is also needed for remote monitoring of patients at home care and for recording data into a patient database. [2–4]

2.2 Microfluidic principles

Point-of-care applications are more and more based on microfluidics [5–7]. Size of these devices has become smaller and smaller during time and so has also the amount of fluids inside them. Controlling and handling of these small amounts of fluids is called microfluidics and in this section the basic principles of microfluidics are introduced.

2.2.1 Fluid and scaling effect

There are three states of matter: solid, liquid and gas. In the solid state matter is tightly packed together through molecular interactions and they have a strict lattice structure. For liquid and gas these interactions are much weaker and thus they do not have a strict order which would keep them in shape. These two states are together called fluids and they can be deformed by applying shear stress on them. [8]

When scaling down the dimensions of a fluidic channel by ten, surface area is decreased by a factor of 10^2 and volume is decreased by 10^3. This means that a surface to volume ratio is increasing when dimensions are getting smaller. When the surface to volume ratio is increased enough, surface related physics are coming dominating over macro

world physics. Conventional fluid physics does not apply and thus microfluidic principles are used. [8]

2.2.2 Surface tension

Surface tension is a liquid property where adhesive and cohesive forces on the liquid gas interface cause the surface to bend. In a bulk solution molecules are surrounded by other molecules and they are equally affecting each other. In the interface gas molecules are less dense and thus liquid molecules tend to draw interfacial liquid molecules inward. Surface tension, γ, is usually presented as a force per unit length or energy per unit area. [8]

2.2.3 Contact angle

When a droplet of liquid is placed on the surface, it has a certain contact angle at a line between wetted and non-wetted surface. In two dimensions, the contact line is presented as a point and the contact angle (Figure 2.1) at this point can be calculated by Young's equation:

$$\gamma_{LG} cos\theta = \gamma_{SG} - \gamma_{SL} \quad (2.1)$$

Where γ_{LG}, $\gamma_{SG}$and $\gamma_{SL}$are surface tensions at liquid gas, solid gas and solid liquid interfaces, respectively. θ is the contact angle. [8]

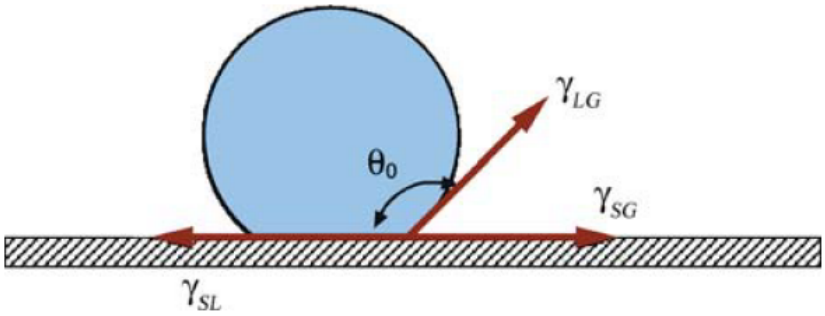

Figure 2.1 *Droplet on a hydrophobic surface. Static contact angle is reached when surface tension forces are at balance along the solid surface. Figure from [9].*

The contact angle is used for characterizing surface wettability and hydrophobicity. When it is over 90 ° for aqueous liquids, the surface is considered hydrophobic and non-wettable. On the contrary the surface with the contact angle less than 90 ° is said to be hydrophilic and wettable. [8; 9]

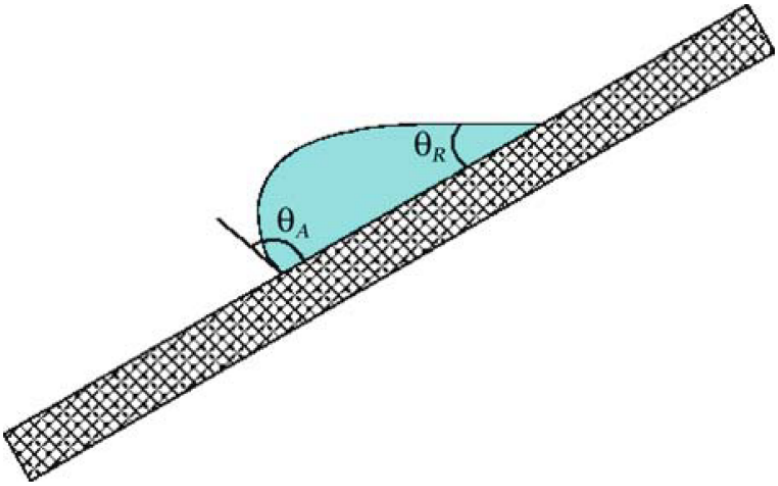

Figure 2.2. *Advancing and receding contact angles characterize surface properties more accurately compared to static contact angles. Figure from [9].*

Dynamic contact angles (Figure 2.2), advancing (θ_A) and receding (θ_R) contact angles, are measured by moving a droplet on a tilted surface or in the liquid channel. In this case there is hysteresis between the contact angles because an advancing meniscus of the droplet is moving towards dry, non-wetted surface and a receding meniscus is moving on the surface which is already wetted by the droplet itself. Hysteresis can be used to characterize surface properties like roughness, mobility and heterogeneity. [8; 9]

2.2.4 Capillarity

Capillarity phenomenon is usually explained with a rising liquid column inside a glass capillary but it also affects fluid flow in all microfluidic channels. The rising of the liquid column occurs due to contact forces between liquid and solid. Also cohesive forces causing the surface tension are included. The liquid column has a certain length when rising stops. In this equilibrium state forces at the contact line are in balance. Gravity of the liquid column has an effect on this height. In smaller channels, gravity has smaller effect than in a wider one and thus liquid rises more in the smaller channel. [10]

In microfluidic channels capillarity can be exploited in controlling a fluid flow. The more hydrophilic surfaces the higher the capillary force is. In this case capillary force acts as fluid driving force causing fluid to flow inside the channel. On the hydrophobic surfaces, capillary force has an opposite effect and it prevents liquid from filling the channel. These physical properties can be used to act as a passive valve where capillary force prevents fluid flow due to the hydrophobic surface or due to sharp corners. The contact angle is used to characterize the strength of capillary force. [10]

2.2.5 Flow control

In addition to capillary force, fluid flow can be generated with electro osmotic flow (EOF) [11] or with pressure [12]. Capillarity is used in paper-based [13] devices but recently developed digital microfluidic systems[14] exploit it by changing the wetting properties of the surface by electrodes.

In EOF, channel walls are negatively charged and thus attract opposite charges from the bulk solution. An electrical double layer is formed and there is a higher density of charges near the wall compared with the middle of the channel. Thus, potential is decreasing when moving from the wall to the center of the channel. If an electric field is applied between channel ends, it will cause electrical force which begins to move positive charges towards a negative electrode. [8; 11]

Pressure difference is the most traditional fluid control method. It can be easily applied either to single phase flows or two phase flows just by adding higher pressure on the inlet than on the outlet.

Navier-Stokes equation is momentum balance equation used to predict fluid behavior:

$$\rho \frac{d\boldsymbol{v}}{dt} = -\nabla p + \rho \boldsymbol{g} + \mu[\nabla^2 \boldsymbol{v} + \frac{1}{3}\nabla(\nabla \cdot \boldsymbol{v})] \tag{2.2}$$

Where ρ is the density of the fluid, $\boldsymbol{v}$ is the velocity vector, t is time, p is pressure, μ is the dynamic viscosity of the fluid and $\boldsymbol{g}$ is the gravity vector. As fluids are many times assumed to be incompressible (constant ρ) Newtonian fluid (constant μ) the equation is simplified to form:

$$\nabla \cdot \boldsymbol{v} = \boldsymbol{0} \tag{2.3}$$

$$\rho \frac{d\boldsymbol{v}}{dt} = -\nabla p + \rho \boldsymbol{g} + \mu \nabla^2 \boldsymbol{v} \tag{2.4}$$

For very slow fluid motion in a micro channel this equation simplifies further to

$$\nabla p = \mu \nabla^2 \boldsymbol{v} \tag{2.5}$$

As the first derivative can be neglected due to slow velocity and gravity is neglected because of a small volume. [8; 12] A constant pressure drop inside the channel with a flow rate, Q, can be described with equation:

$$\Delta p = R_{hyd} Q, \;\; R_{hyd} = \frac{8}{\pi} \mu L \frac{1}{{r_{cha}}^4} \tag{2.6}$$

Where R_{hyd} is the hydraulic resistance of a channel. The hydraulic resistance of a circular channel is given as an example. r_{cha} is the radius of the circular channel and L is the length of the channel.

2.2.6 Plug flow

In plug flow, the channel contains at least one plug of liquid which is separated by another liquid or gas (Figure 2.3). Pressure can be used to move this liquid plug, but in addition to fluid friction there is also capillary force affecting both ends of the plug. Thus total pressure drop in the channel is

$$\Delta p_{channel} = \Delta p_{drag} + \Delta p_{cap} \tag{2.7}$$

Pressure drop due to fluid friction for the circular channel is written as

$$\Delta p_{drag} = \frac{8v}{{r_{cha}}^2}(\mu_1 L_1 + \mu_2 L_2) \tag{2.8}$$

Where v is the average velocity of the fluid, r_{cha} is the radius of a circular channel, L_1 and L_2 are total lengths of the plugs of fluid 1 and 2. μ_1 and μ_2 are dynamic viscosities of the fluid 1 and 2.

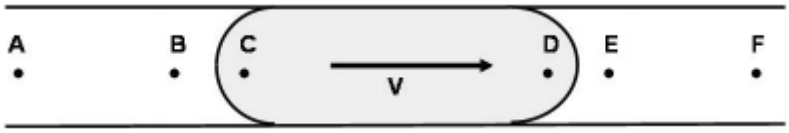

Figure 2.3. *In plug flow friction forces are affecting inside the fluid (between A-B C-D and E-F) and capillary forces between surfaces (B-C and D-E) [15].*

Capillary force is acting on the plug interfaces and magnitude of the pressure drop is related to contact angles on the advancing, θ_A, and receding meniscus, θ_R, as

$$\Delta p_{cap} = \frac{2\gamma}{r_{cha}}(-cos\theta_A + cos\theta_R) \tag{2.9}$$

Where γ is the surface tension at interfaces Pressure always decreases from inlet to outlet but over the receding interface it may temporarily increase when the receding contact angle is more than 90°.[15]

2.2.7 Laminar flow

Reynolds number (Equation 2.10) characterizes the quality of the fluid flow. It represents the ratio between inertial forces to viscous forces in the fluid.

$$Re = \frac{\rho v D_{hyd}}{\mu},\ D_{hyd} = \frac{4A}{P} \tag{2.10}$$

Where ρ is the density of the fluid, v is the average flow velocity in m/s, μ is the dynamic viscosity of the liquid and D_{hyd} is the hydraulic diameter of the channel. A is the cross sectional area of the channel and P is the perimeter of that area. When the Reynolds's number is less than 2000, fluid flow is considered fully laminar. Between 2000 and 4000 is the transition stage and above 4000 flow is fully turbulent. [8] For example, the channel used in the thesis is 0.5 mm high, h, and 2 mm wide, w. The highest flow rate used in the channel is 3.25 ml/min. When water at 20°C temperature is flowing through the channel, Reynolds number is approximately 43.

Scales of microfluidic systems are so small that fluid flow is fully laminar. In laminar flow, fluid is flowing in layers along each other parallel to walls. In this kind of flow lateral mixing is mainly diffusion based. [8]

2.2.8 Diffusion

Diffusion is a mass transfer phenomenon which occurs due to the random Brownian motion of the molecules. In gas or liquid, molecules vibrate and move straight until they collide with other molecules. On a collision molecules change the direction until they collide again. Although bulk solution does not seem to move, molecules inside it are moving randomly all the time. This temperature dependent vibrational movement is the physical explanation for diffusion. [16]

A fundamental example of diffusion is bulk solution which is divided with a non-permeable membrane and each side of the membrane has different concentration (the amount of substance in unit volume [mol/l] = [M]) of molecules. When the non-permeable membrane is removed, molecules are unevenly distributed in the bulk solution. A concentration gradient is formed at the place where the membrane was removed. After some time, molecules spread due to the Brownian motion to cover the whole bulk solution and distribute evenly over the whole volume. During this process, the concentration gradient widens and in the end disappears. [16]

To describe this gradient based molecular movement Adolf Fick developed Fick's law for one dimensional flux $\boldsymbol{N_i}$ as

$$\boldsymbol{N_i} = -D_i \frac{\partial c_i}{\partial x} \tag{2.11}$$

Where $\boldsymbol{N_i}$ is flux per unit area, c_i is concentration, x is distance along axis x and D is the diffusion coefficient. In three dimensions, Fick's law is presented as

$$\boldsymbol{N_i} = -D_i \nabla c_i \tag{2.12}$$

This can be explained in the following way. Flux will occur in a direction of the negative gradient (from higher to lower) of concentration with the speed of a diffusion coefficient D. First law is used to derive Fick's second law to present time dependent change in concentration

$$\frac{\partial c_i}{\partial t} = D_i \nabla^2 c_i \tag{2.13}$$

The diffusion coefficient is a natural constant which is dependent of the molecule or particle. There are many estimates for it but maybe the most common one is Stokes-Einstein equation

$$D_i = \frac{k_B T}{6\pi\mu r_i} \tag{2.14}$$

Where k_B is Boltzmann's constant, T is the temperature in kelvins, μ is the dynamic viscosity of the solvent and r_i is the radius of the solute. This equation is used to estimate the diffusion coefficient for spherical molecules which are much larger than comparison with the molecules of the surrounding solvent. [16] Diffusion distance, d, can be written as

$$d = \sqrt{D_i t} \tag{2.15}$$

Here t is the diffusion time. This means that a particle which has the larger diffusion coefficient will move faster over a certain distance. Diffusion limits the mixing speed and thus small dimensions are favorable to ensure fast chemical reactions. Different micro mixer structures and methods have been developed to overcome limitations caused by the diffusion in the micro scale. [16; 17]

2.3 Immunoassay

Immunoassays are analytical methods used to detect an analyte and to quantify the concentration of it. Immunoassays have been used widely in in vitro diagnostics for their simple structure, rapid and sensitive detection for versatile analytes. There are several different immunoassays. Immunoassay can be homogeneous or heterogeneous, competitive or non-competitive and there are several different detection methods. A structure and a detection method of different assays may vary but all immunoassays have one common element: they all exploit specifically binding antibodies (Ab).

2.3.1 Antibodies and antigens

Antibodies are proteins produced by a living creature. Immune system uses these proteins to recognize different types of antigens (Ag) inside the body. If a foreign antigen is detected, the immune system begins to produce more antibodies against this foreign “pathogen” and tries to prevent it from spreading and causing disease. There are several types of antibodies produced inside the body and immunoglobulin G (IgG) is the most abundant. [18]

The basic structure of an antibody (Figure 2.4) is usually described as a Y-shape protein of four polypeptide chains. It has two similar heavy chains and two similar light chains, which are bound together through disulphide bonds. These chains can be further divided into constant and variable domains depending on amino acid variability. [18]

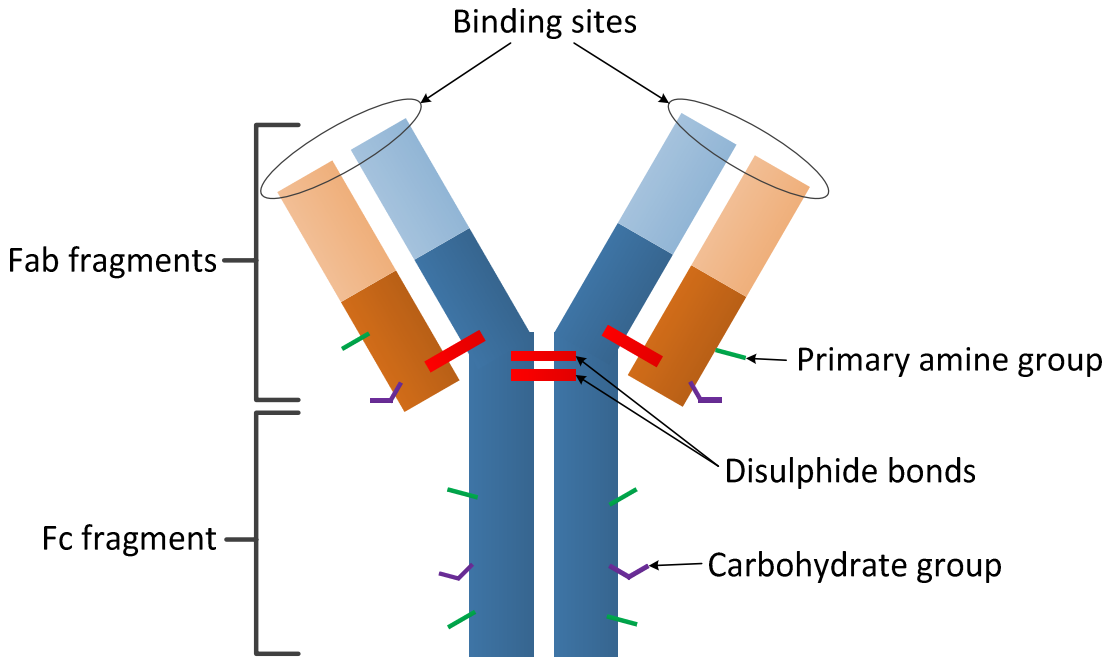

Figure 2.4. *The structure of an antibody. Two heavy chains (blue) and two light chains (orange) are bound together with disulphide bonds (red). The antibody has two Fab-fragments and one Fc-fragment. Constant domains are colored with dark and variable domains with light color.*

Variable domains on N-terminus of the peptide chains are part of the antibody binding fragments (Fab), which are key regions in detecting different antigens. Structure of the fragments enables specific binding to a specific region (epitope) on the antigen. The fragment crystallisable (Fc) part is located in C-terminus of heavy chains and it has an important role in immunological responses after antibody-antigen interaction. [18]

Fab's and Fc regions are the most important parts of the antibody, but there are also some carbohydrate and primary amine groups which can be used for labeling or attaching the antibody on a surface. [18; 19]

2.3.2 Heterogeneous vs. homogeneous immunoassays

The immunoassay methods are divided into two main branches. In homogeneous assays, all molecules are free and all reactions take place in solution. Special labels have to be used in homogeneous assays. The label must be detectable either when the antigen is free or bound on the antibody, but not in both cases. All substances can be mixed together and separation is not needed. This makes homogeneous immunoassays very fast and easy to perform. [20]

In heterogeneous immunoassays antibodies or antigens are attached to the surface and they are used to capture the desired antigen or antibody from the sample. Labels used do not make the difference between binding reactions as in the homogeneous case and thus all excess unbound labels must be separated from the surface by a washing procedure. [20]

2.3.3 Competitive vs. non-competitive assays

The immunoassay methods can be further divided into competitive and non-competitive assays. In the competitive immunoassay, a certain amount of labeled antigen is added to solution with the unlabeled antigen of interest. These antigens compete for limited binding places. The more unlabeled antigen there is the more it will displace labeled antigens. Hence signal will decrease when the analyte concentration is increasing. Competitive immunoassays are usually performed for small univalent analytes having only one epitope. [20]

In the non-competitive immunoassays, the detected signal is directly proportional to the amount of bound antigen. Non-competitive immunoassays demand a sandwich structure: Antigen bounds to capture antibodies on the surface. To detect bound antigens, labeled tracer antibodies are added on the surface on top of bound antigens. Tracer antibodies bind on antigens and form a sandwich structure. In the end, labels are used to measure the number of bound tracer antibodies on the surface and the relation between them and antigen concentration is used to calculate the original amount of antigen in the sample. [20] Non-competitive assays are usually performed with reagent excess. This means that the amount of tracer antibodies and the number of binding places on the surface overcome the number of antigens on the sample. This way the number of bound antigens and the number of tracer antibodies are maximized.

Both heterogeneous competitive and non-competitive sandwich assays can be done either with one step or with two steps. In non-competitive assay which is done in one

step, tracer antibodies and antigens of interest are mixed together with a known amount of capture antibodies. Immunocomplexes, which contains capture antibodies bound to tracer antibodies by the antigen, are formed and measurement is done after washing all unbound labels away. In two steps assay, the antigen of interest forms the first immunocomplex with capture antibodies and all unbound antigens are washed from the surface. In the second step, tracer antibodies are added to surface to form the full immunocomplex. After this, the surface is again washed to remove all excess labels from the surface. Two step assay formats usually provides higher sensitivity and specificity compared with one step assays. [20]

2.3.4 Basic immunoassay reactions and reaction rates

Antibody binding can be described as a chemical reaction where the separate antibody and antigen are reactants and form an antibody-antigen complex as a final product. For the simple case where the antibody has only one binding place the reaction can be written as:

$$Ab + Ag \underset{k_d}{\overset{k_a}{\rightleftarrows}} AbAg \tag{2.16}$$

Where Ab is the antibody, Ag is the antigen and AbAg is antibody-antigen complex. Two sided arrows indicate that the reaction can occur in both directions. In other words, reaction is reversible. [21]

A reaction rate is a definition how much the concentration of certain reactant or product is changing as a function of time. The concentration of bound analyte is measured in immunoassays and thus reaction rate for antibody-analyte complexes is an important factor which has to be taken into account when designing immunoassays. This reaction rate, R, can be derived from the reaction equation:

$$R = \frac{d[AbAg]}{dt} = k_a[Ab][Ag] - k_d[AbAg] \tag{2.17}$$

The concentration of a substance is marked with square brackets. Parameters, k_a and k_d are reaction rate constants for association and dissociation reactions, respectively. Reaction rate constants tell how fast reactions occur when reagents collide. Collisions are related to the concentrations of the substances and thus they are also included in the equation. The reaction rate equation can be explained by the following way. First part comes from an association reaction where complexes are formed depending on the concentrations of antigens and antibodies. Second part is for a dissociation reaction where complex is taken apart and thus it has a minus sign. [21]

Reaction rates are used for modeling chemical reactions and two parameters which can be easily studied are initial reaction rate and steady state approximation. At the beginning of the reaction there are only initial concentrations for antibodies and analytes, $[Ab]_0$ and $[Ag]_0$ respectively. The concentration of complexes is zero and thus the initial reaction rate, R_0, can be written as:

$$R_0 = \frac{d[AbAg]_0}{dt} = k_a[Ab]_0[Ag]_0 \tag{2.18}$$

In a steady state there occurs reactions both directions all the time but they occur at the same rate and thus it seems that nothing is happening. The system is in equilibrium and the total reaction rate is assumed to be zero. The steady state approximation is used to estimate the final concentrations of different compounds:

$$R = \frac{d[AbAg]}{dt} = k_a[Ab][Ag] - k_d[AbAg] = 0 \tag{2.19}$$

$$k_a[Ab][Ag] = k_d[AbAg] \tag{2.20}$$

$$K_A = \frac{k_a}{k_d} = \frac{[AbAg]}{[Ab][Ag]} \tag{2.21}$$

Where K_A is an association constant. Dissociation constant, K_D, is an inverse of the association constant. These are reaction rate parameters which are usually provided by antibody producers. [21]

2.4 Interferences in immunoassay

Immunoassays are effective tools for measuring analyte concentrations from the bodily fluids, but there are several interferences which may cause erroneous results. In this section, these interferences are shortly introduced and basic procedures for avoiding them are presented.

2.4.1 Unspecific binding of the label on the surface

Even though there are no antigens in the sample a small number of the label particles will stick to the surface. This phenomenon is called unspecific binding. These unspecifically bound labels lead to a higher noise level and usually also to a higher deviation of the noise. Thus unspecific binding is reducing a signal to noise ratio and more important, causing a higher limit of detection for the assay. There are several reasons why unspecific binding occurs. First, adsorption can occur straight to an exposed material surface. To prevent this surfaces are usually modified with self-assembling monolayers or some strong adsorbing protein which would form a

protective layer against unspecific adsorption. Second, it is possible that capture antibodies on the surface bind to the tracer antibodies. Reason for this may partially be in carbohydrate and amino groups of the antibodies. Third, the surface may have a structure or shape which fastens the label on the surface. [22; 23]

2.4.2 Hook effect

If the measurement signal is presented as a function of concentration, the signal usually rises due to bound labels. After a certain concentration, the signal starts to decrease and forms a hook. This is called the hook effect and it is caused by an antigen excess in the system. Antigen molecules bind to capture antibodies and labeled antibodies. When there are enough antigens all binding places from both the capture and label antibodies become filled. Thus the label antibodies do not bind as efficiently to the capture antibodies and the measured signal decreases as the antigen concentration increases. [23; 24]

Erroneous results caused by the hook effect can be avoided by a couple of means. Usually the sample is diluted enough to be certain that the concentration is on the rising side of the hook. This can be done when the sample is well known and usual concentration values are familiar. On the opposite it is possible to use reagent excess of antibodies to be sure that binding sites will not come saturated. Last method is to perform the assay in two steps using washing between antigen incubation and label antibody incubation. [23; 24]

2.4.3 Cross reactive substance

Antibodies are not perfectly specific for certain antigens. There may be substances in the sample which have similar structures as the antigen which is wanted to measure. In this situation, antibodies cross react with these molecules and cause distorted results. This is mostly causing problems in competitive immunoassays due to an extra competitor. Sandwich assays are more specific as there are two different antibodies which are binding to the antigen. As antibodies are binding at the same time it is less probable that both of them can bind to a substance other than the antigen. [24]

2.4.4 Anti-animal antibody interference

Blood contains several antibodies which can either react with antibodies used in the assay or with the measureable antigen and thus cause interference in the immunoassay. Human anti-animal antibodies (HAAA) are able to recognize animal antibodies with high specificity. HAAAs can bind either to a constant or a variable part of the animal antibody. If animal antibodies are used as capture or tracer antibodies, it is possible that HAAAs attach to them and prevent antigen or tracer binding on the surface. This leads to a false negative result. On the other hand, if HAAAs are able to bind to both tracer and capture antibodies, the result is false positive. Interferences are mainly avoided by

carefully planning the assay design and what kinds of antibodies are used in it. Other way is to remove HAAAs by a sample pre-treatment. [25]

2.4.5 Matrix effect

Immunoassays are quite sensitive to the environmental conditions of the sample, also called a matrix of the sample. Ionic strength, pH and protein and lipid concentrations of the sample are affecting the reactivity of antibodies. Composition of the blood varies a lot between different people and thus matrix effect may cause different results for different people. Matrix effect is minimized by diluting the sample in the buffer solution. This way, environmental factors are tried to be kept constant for every sample. [24]

2.5 Detection methods

There are several different detection methods for immunoassays which can be divided in to two main categories: techniques which use labeled molecules for detection and techniques which are label-free.

First immunoassays used radio-isotopic labels (radio-isotopic immunoassay or RIA) [26]. These labels have some disadvantages and they have been replaced by labels like fluorophores in fluorescence immunoassays (FIA) and by enzymes in the enzyme linked immunosorbent assays (ELISA). FIA and ELISA are nowadays two most used detection methods. New labels are developed all the time and especially the use of quantum dots and nanoparticles is increasing. [27] In this thesis, a time-resolved fluorescence method was used as a detection method for the immunoassay. Basics of the method are explained in the next section.

Label-free detection methods are typically based on the change of mass over a specific surface. There are several different method to detect the change in the mass like surface acoustic waves [28], piezo resistive cantilevers [29] or a surface plasmon resonance [30].

2.5.1 Time-resolved fluorescence

Fluorescence is the form of luminescence where molecules are excited with the photons having a certain wavelength. In excitation, the energy of the photon is adsorbed by an electron that jumps from a lower energy level to a higher one. Because electrons tend towards a minimum energy state, the electron soon returns to a lower energy level where it originally was. Usually, the electron returns to a lower level in two phases. First it goes through non-radiating transition where part of the gained energy is lost as heat. In the second phase there occurs a radiating step where the rest of the energy is released as a photon. As part of the excitation energy is lost in the non-radiating

transition, the emitted photon has lower energy and thus also longer wavelength than the exciting photon.

Traditional fluorophores usually have a very short emission lifetime, less than 100 ns. In time-resolved fluorescence a special type of fluorophores are used. Some lanthanide chelates, like Europium(III), Dysprosium(III),Terbium(III) and Samarium(III), have a very long emission lifetime spanning from 10 to 100 µs. This ensures that background fluorescence from excitation light is already diminished when the actual measurement is done (Figure 2.5). This way most of the measured signal is caused only by the labels, which afford high sensitivity to the measurement. [31; 32]

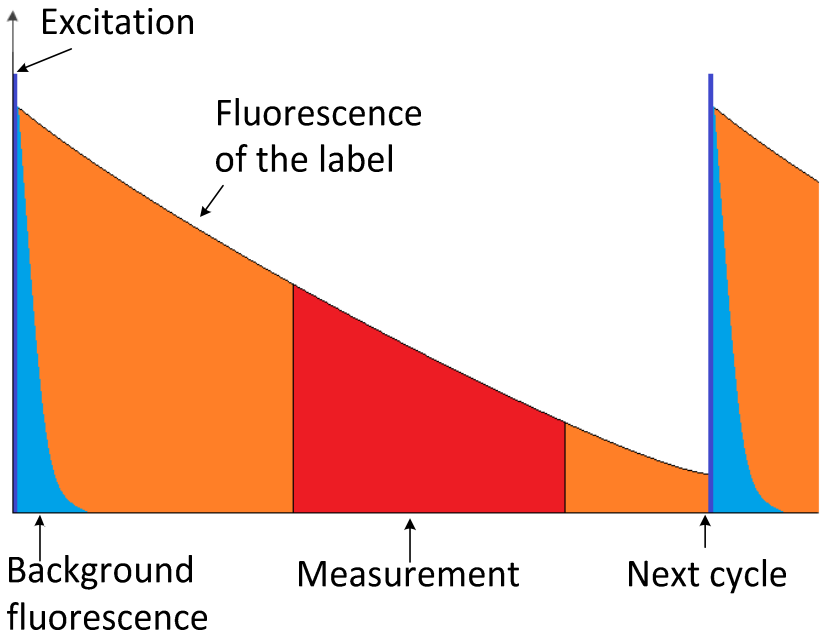

Figure 2.5. *The basic principle of the time-resolved fluorescence measurement: The sample is first excited with a certain, high energy, light pulse. A photon count measurement is done from a certain time interval after background fluorescence is diminished.*

Other advantage of the lanthanide chelates is a large stokes shift. The Stokes shift means the difference between the excitation and the emission wavelengths. With traditional fluorophores excitation and emission wavelengths are overlapping. Due to this, the separation of these wavelengths using optical filters is challenging. With lanthanide chelates, the stokes shift is larger and there is no overlapping between excitation and emission wavelengths. This makes the separation easier than with traditional fluorophores. [31; 32]

Lanthanide chelates (Figure 2.6) are compounds where a lanthanide ion is bound to an organic chromophore via metal binding groups (chelators). Lanthanide ions are difficult to excite directly. Instead, of exciting lanthanide ions, the organic chromophore is used

to adsorb excitation energy. Energy is transferred to the lanthanide ion which then emits photons with narrow bandwidth. Chelates are sensitive to the environment and for example water and some heavy metals [33] are known to quench their fluorescence signal. In quenching, the excitation energy is transformed fully to heat and thus photons are not generated. [34; 35]

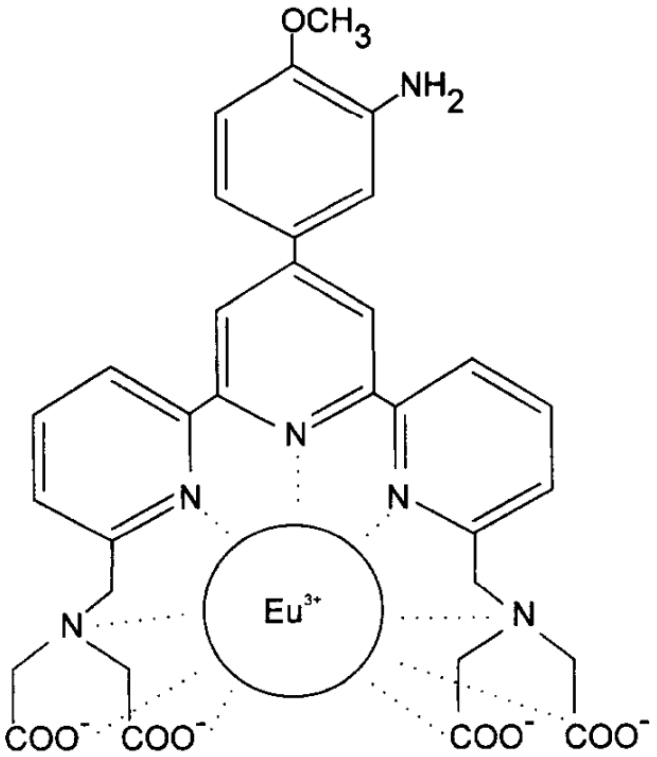

***Figure 2.6**. Example of an europium(III)-chelate. Eu(II1) 4'-(3-amino-4-methoxyphenyl)-6,6"-bis(N,N-bis(carboxymethyl)aminomethyl)-2,2': 6',2"-terpyridine. Figure from [35]*

2.5.2 Europium nanoparticles

In europium nanoparticles, chelates are embedded inside a polystyrene shell. The first advantage of the shell is that it protects the chelates from environmental effects and this way prevents quenching. Secondly, it is possible to have several thousand chelates inside a single nanoparticle. This way the label provides a much higher intensity compared with a single antibody which does not have as many chelates. [34]

The polystyrene shell itself contains carboxylic acid groups which can be used to couple antibodies on the surface of the nanoparticle [36]. Doing so it is possible to increase binding places on the particle and thus nanoparticles have increased reaction rates [37]. With these properties europium chelate nanoparticles has shown to have high sensitivity over individually labeled antibodies.

2.6 Parameters affecting assay performance

This section discusses the evaluation of immunoassay performance and presents parameters related to the immunoassay performance. Sensitivity is one of the most used terms when speaking about assay performance. Unfortunately, it has many meanings and thus it might be used in a confusing way. Thus, different definitions of sensitivity are discussed first.

2.6.1 Sensitivity

There are three different kinds of sensitivities which are used when speaking about immunoassays: measurement sensitivity, analytical sensitivity and clinical sensitivity. As all of these have completely different meanings it is important to know the difference between them.

Measurement sensitivity is commonly used in the field of measurement technology. [38] It is used to describe how measurement result changes within the linear range of the measurement (Figure 2.7). In other words, it is the slope of a measurement curve in the linear range:

$$Sensitivity = \frac{\Delta Signal}{\Delta Concentration} \tag{2.22}$$

Further on in this thesis the term sensitivity refers to the measurement sensitivity.

The second term is analytical sensitivity which is also called a limit of detection (LOD). It defines the smallest amount of concentration which can be detected with a measurement device. [39] It is calculated as:

$$LOD = \frac{3\sigma_N}{Sensitivity} \tag{2.23}$$

Here σ_N is the standard deviation of the signal noise. This equation gives 99.87% confidence that LOD value is not a part of the noise. Further on in this thesis, LOD is used to avoid confusion with the measurement sensitivity. [39]

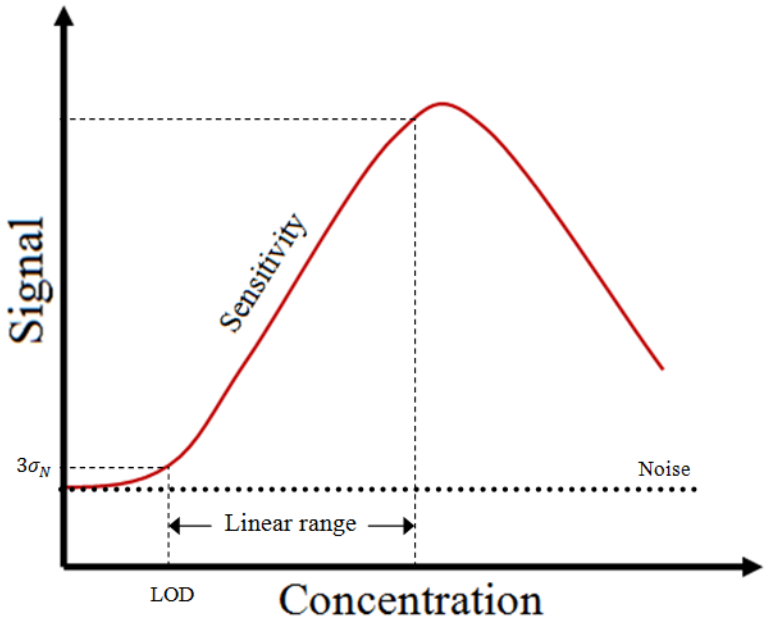

Figure 2.7. *Signal to concentration of a measurement to clarify the difference between sensitivity and limit of detection. Hook effect can be seen after linear range.*

Clinical sensitivity is the term used in clinical studies. It is statistical value which describes how well the test will correctly identify diseased patients [40]:

$$Clinical\ sensitivity = \frac{True\ positive}{True\ positive + False\ negative} \tag{2.24}$$

True positive means that a patient has disease and the test result is positive. False negative means that a patient actually has the disease, but the test result is negative. As the cartridge is still in a development phase this parameter is not yet needed.

2.6.2 Material and surface roughness

Material properties have a big effect on how proteins are adsorbed on the surface. Proteins have regions which can interact with the material surface by many means like hydrophobic or hydrophilic interactions or through positive or negative charges etc. [41] These interactions not only define how proteins stay on the surface as they have been adsorbed but also how they maintain their structure. This is important as heterogeneous immunoassays are relying on coatings which can specifically capture the certain antigen. It is important to have a high capacity surface where antibodies are aligned correctly and retained their functionality to capture the antigen. Such a surface offers a lot of specific binding places for the antigen and leads to higher signal values.

In addition to the material, the roughness of the surface also affects adsorption and protein folding. Additional to this the total surface area can be increased with micro and

nanostructures. This way the amount of binding places on the surface can be increased which leads to higher fluorescence signals. [42; 43]

2.6.3 Reaction time

Immunoreactions eventually reach the steady state situation where as many binding reactions as detaching reactions happen. In this balance situation the maximum number of antigen bindings is reached and thus the signal values are the highest. Unfortunately reaching this situation normally takes several hours.

In point-of-care applications results are desired as soon as possible. Using shorter times means that the reactions are stopped as they are still going on. Thus the signal levels of the result are lower than with assays where the steady state is reached. This affects the overall performance of the assay as the measurement sensitivity is lower. Deviation in assay time also has a more significant effect on signal values in short time incubation compared with a longer incubation.

2.6.4 Temperature

The temperature affects molecular vibrations. In higher temperature, more molecules will vibrate. Diffusion is based on random vibrations and thus the temperature influences the diffusion coefficient (Equation 2.14).

Reaction rates also depend on the temperature as more vibrations means that there will be more collisions between molecules and thus more possibilities for reactions to occur. Unfortunately, as antibody reactions are reversible also dissociation reactions are affected by the temperature. Thus it is not so straightforward to say how the temperature affects reaction rates. Increase in the temperature increases antibody activity, but high temperatures will cause denaturation and molecules lose their functionality [44]. In this thesis, the temperature is not studied as it was seen best to mimic the nature and use 36 °C temperature.

2.6.5 Concentrations

Concentrations have an effect on the overall assay through reaction rates. The more there are initial substances the more equilibrium will move towards the end products. Most of the immunoassays rely on a reagent excess. This way, most of the antigens will react with label and capture antibodies. Usually the density of specific binding places is maximized to reach high reaction rates and signal values.

The only drawback in the reagent excess method is that as there occur nonspecific binding on the surface the number of label molecules have to be optimized. If there are too few labels, it means that signal levels would not be as high as with higher label

concentrations. On the contrary if label concentration is too high unspecific binding will occur and thus the noise level increases.

2.6.6 Shape of the reaction chamber

A shape of the reaction chamber in a microfluidic cartridge defines the amount of the sample which can be used. If the immunoassay is performed using stationary incubation, the assay will be diffusion limited. Thus it is useful to know how large volume is reasonable to perform accurate measurement.

More important is the fluid flow through the chamber. If there are any bubbles generated inside the chamber, they may prevent immunoreactions from taking place or prevent the proper washing of the excess labels. In both cases the final results will be erroneous.

2.7 Finite element method modeling

The finite element method (FEM) is a numerical technique used to discretely approximate solutions for partial differential equations (PDEs). PDEs are represented in a matrix form which is solved depending on applied loads. The finite element method was first used in structural mechanics but in this case a microfluidic system is used as an example. Given description is a very simplified version of the whole process. More detailed information of the FEM can be found in the book “The finite element method” written by Zienkiewicz and Taylor [45; 46].

In the FEM modeling a system is presented with geometry. The geometry is divided into smaller elements (Figure 2.8), which are connected to each other via nodes. These nodes are used for creating a stiffness matrix for a model in such way that a node is basically affected only by its neighbor nodes in certain manner. The effect of the neighbor node is described with PDEs of the studied physics and node positions are taken in to account in forming final equations which describe the system. In a fluidic system Navier-Stokes equation (Equation 2.2) would be used to describe fluid flow. [45; 46]

The way domains in the geometry are defined is called domain conditions. As there can be more than one material inside the geometry there can also be multiple subdomains where physics are defined in a different way. For example, in the plug flow the geometry will contain domains for gas and liquid materials.

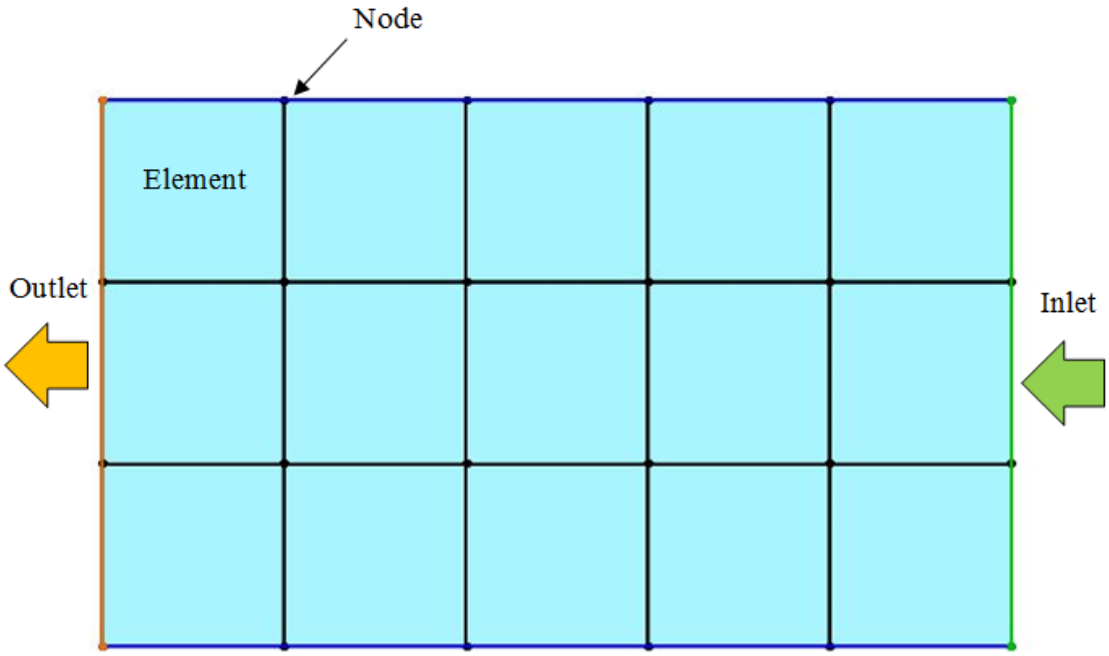

Figure 2.8. *Basic idea of FEM. Boundary conditions are marked with different colors.*

As the system is finite, it has some boundaries. These boundaries have to explain the relation between the system and the outside of the system. These relations are called boundary conditions. For example, when modeling a fluid flow through the system one has to define an inlet, an outlet and walls for the system. All the nodes in the inlet boundary have to be defined in such a way that matter can flow in to the system. If nodes on walls are defined to be rigid and non-permeable, the model should also have the outlet for the matter. This way an impossible situation where infinite amount of matter would fill the finite volume is avoided.

The basic idea of the FEM is that solution is gained through matrix calculation where a displacement matrix, **a**, is solved related to a stiffness matrix, **K**, and applied loads or external force **r**:

$$\boldsymbol{Ka = r - f} \tag{2.25}$$

In here $\boldsymbol{f}$ stands for forces needed to balance the distribution of load force and initial strains over elements. For the fluid flow example, the load means pressure on the inlet and the outlet. Pressure difference will cause the certain fluid flow rate inside the system. In this case the displacement matrix would present a velocity field of the fluid inside the system. [45; 46]

In most FEM software, all models are created through the same basic steps:

1. Create a geometry
2. Define domain and boundary conditions
3. Mesh geometry
4. Solve the system
5. Post process the results

The first step is to draw the geometry or importing it to software from a separate file. In the second step the user defines domain conditions. This means setting correct material parameters for the geometry. In chemical models, domain conditions define concentration and the diffusion coefficient etc. In the same step one defines how different boundaries act. Where are the walls, inlets and outlets. In other words, these are loads applied to the system.

The third step is meshing, where the geometry is divided into smaller pieces. Elements and nodes are used to assembly the stiffness matrix. The challenge in meshing is to reach balance between model accuracy and simulation time. The denser the mesh is the more accurate results are gained. On the contrary, if mesh is too dense it will result in the large stiffness matrix and thus it will take more time to solve the system. In some cases it is even possible that a computer run out of memory due to large matrices. A smaller mesh is easier to solve but it will generate a less accurate result. In the end, model is solved and results are post processed to presentable form. [47]

3 MATERIALS AND METHODS

This chapter presents all the practical work done for the thesis and all the equipment used to fulfill different tasks. First, cartridge geometries and fabrication methods are described. Second section explains the coating of the immunoassay surfaces and experiments done with them. Third section explains the used models.

3.1 Cartridge for immunoassay

Thyrotropin (TSH, thyroid stimulating hormone) immunoassay was used as a model assay due to the fact that TSH is a quite well known analyte. Cartridge fabrication and antibody coatings and method to perform immunoassays are explained next.

3.1.1 Used Geometries

Three kinds of reaction chambers are used in the experiments. Chamber 1 is the original chamber of the NanoFlow cartridge (Figure 1.1) which was 12 mm long, 4 mm wide and 0.5 mm high. Volume of the chamber was 40 µl and area of the reaction area was approximately 54 mm^2.

Chamber 2 (Figure 3.1a) is a more simplified one. It is actually just a widened part of a 2 mm wide and 0.5 mm high channel. The chamber is 4.5 mm wide and 14.5 mm long. Height is constant 0.5 mm. The volume of the chamber is 27 µl and the reaction area is 68.08 mm^2. This chamber is used in material comparison.

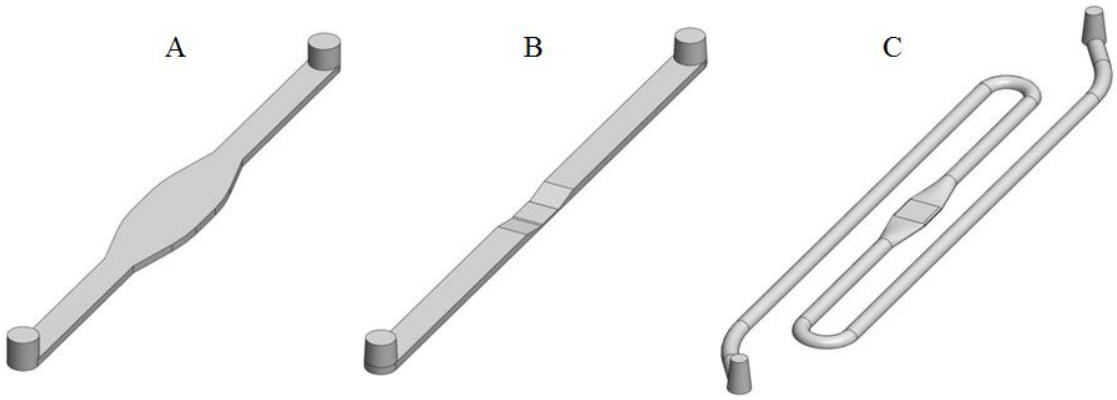

Figure 3.1. *The structures of the reaction chamber inserts used in the thesis.*

Chamber 3 (Figure 3.1b) is designed as a result of the FEM models. Instead of having a reaction chamber with large volume, a narrowing in the channel is used as the reacting

surface. The narrowing was 6 mm long where 2 mm of the middle has a constant height of 150 µm. The chamber has small 50 µm barriers at the beginning and at the end of the reaction area. Purpose of these barriers is preventing coating solutions spread in the channel. The reaction area was around 5.1 mm^2. Chamber volume is around 0.8 µl. 16 µl sample is used to fill the whole chamber. The idea of the narrowing is to test the effect of chamber height on the immunoassay with stationary incubation. On the other hand, as the narrowing works as a passive valve, it can be used to control reciprocating flow over the reacting surface. Moving the sample during incubation increase the mass transfer of the particles towards the reacting surface and will lead to higher signal values.

As mentioned earlier, increased surface roughness and microstructures would increase the amount of protein adsorption on the surface. This will be tested by making microstructures in the reaction area of the Chamber 3. Molds for the chamber are done in University of Eastern Finland where micro cavities are laser ablated in the reaction area with a femtosecond laser [48]. These cavities should be replicating to the plastic cartridge as microstructures increasing total surface area and thus increase signal levels.

The Chamber 3 had some problems with capillary effect, which caused bubbles to occur. Thus it had to be modified. For the Chamber 4 (Figure 3.1c), the channel cross-section was changed to a half circular shape which has 0.5 mm radius. To get the same amount of sample to fit inside the channels they were lengthened. Second, the chamber height was increased to 200 µm and barriers were removed. Chamber edges were also rounded with a radius of 100 µm.

3.1.2 Injection molding

Two types of injection molded cartridges are used as a substrate for the immunoassay (Figure 3.2). The NanoFlow cartridge has all microfluidic components while the insert cartridge is used to test an individual component. In this thesis different chamber geometries are used in the insert cartridge. Fabricating new molds is cheaper as only a small part of the mold is needed to change instead of the whole mold.

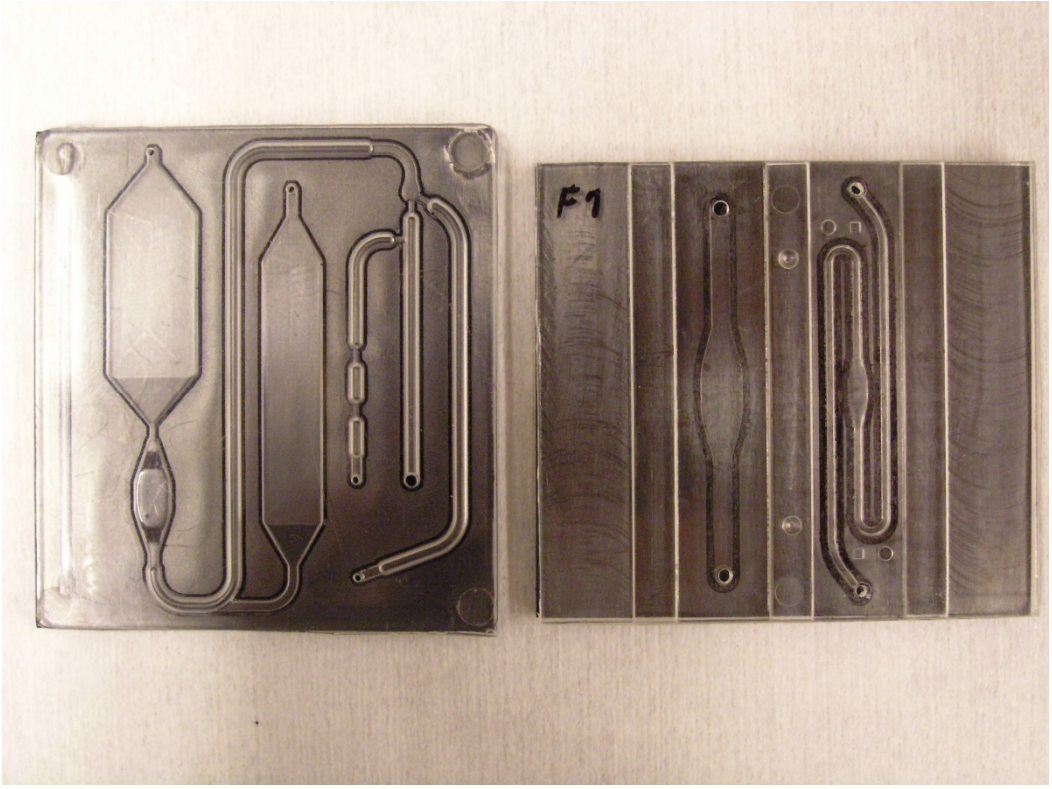

Figure 3.2. *Laser welded cartridges used in the thesis. The NanoFlow cartridge is on the left and one of the insert cartridges containing the Chamber 2 and the Chamber 4 is on the right.*

The NanoFlow cartridges were injection molded from a high-impact polystyrene grade Styrolux 656C (Styrene-butadiene copolymer from Styrolution). Injection molding was done by Plastone Oy (Nurmijärvi, Finland). Injection moldings of the insert cartridges were done in the Polymer laboratory of Tampere University of Technology. Three different PS grades, Styrolux 656C (styrene butadiene copoplymer (CBS) from Styrloution), PS 158K (general purpose PS from BASF) and Empera 124L (general purpose PS from Ineos-Nova) were used in these cartridges. Also a PMMA grade LG PMMA HI 835M (Ides) was used for a comparison. For the Chamber 4 experiments, KR-01 grade SBC (from K-resin) was used as Styrolux 656C was temporarily out of stock.

3.1.3 Reaction chamber coating

The injection molded plastic cartridges were first cleaned by rinsing them in isopropanol, then washed with deionized water and dried with compressed air. In the reacthion chambers, functionalized surface for heterogeneous immunoassays were fabricated in three steps.

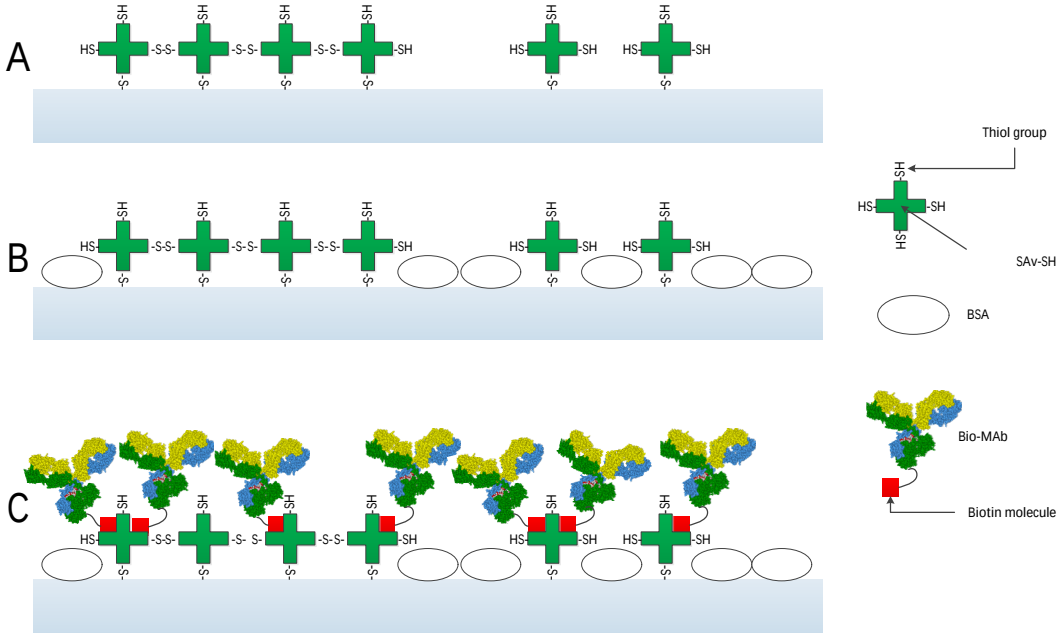

Figure 3.3.*The basic fabrication steps to make the specific coating on the reaction chamber.*

In the first step thiolated streptavidin (SAv-SH) [49] from the Department of Biotechnology at the University of Turku was adsorbed on the surface by dispending 80 µl of SAv-SH solution (1000 ng/40 µl) in the reaction chamber. The solution was incubated in a humid box at 36 °C overnight. SAv-SH surface was washed with 1 ml of 1×DELFIA® washing solution (PerkinElmer-Wallac Oy, Turku, Finland) which contained 0.05 g/l of Tween20 detergent (Merk).

The next step was to adsorb bovine serum albumin (BSA)-molecules on the surface to fill empty gaps left by the streptavidin to prevent unspecific binding onto the surface. This was done by dispending 80 µl of saturation solution (containing 50 mM Tris-HCl, pH 7, 150 mM NaCl 0.5 g/l NaN_3, 60 g/l D-sorbitol and 2 g/l BSA) in the reaction chamber and incubating it overnight in the humid box at room temperature.

In the last step the saturation solution was sucked out from the chamber and biotinylated antibodies (Bio-MAb Anti-TSH 5405) were attached to SAv-SH, via biotin-streptavidin linkage, by incubating 80 µl of antibody coating solution in the chamber at room temperature for 2 hours. Coating solution contained 200 ng/40 µl antibodies in Kaivogen buffer solution (Kaivogen Oy, Turku, Finland). Finally antibody coating solution was washed with 1 ml of 1×DELFIA® washing solution.

3.1.4 Laser welding

As the injection molding leaves microfluidic channels open they must be sealed properly before fluid handling. This was done by covering the cartridge with a black cover plate and welding these parts together with a laser (Figure 3.2). Laser welding

method is presented more accurately elsewhere [50]. Shortly, laser is used to heat the black cover plate through the transparent cartridge. Raise in the temperature mainly occurs on the interface between the plastics thus melting them together. Coated cartridges were stored at 4 °C in minicrip bags in a fridge before and after the welding process.

Laser welding was done at the Department of Production Engineering (Tampere University of Technology). The used materials were commercial extruded PS-sheets, Vikureen (Athlone Extrusions, Ireland), NUDEC PS-sheet (NUDEC, Spain) or injection molded plates which had the same materials as cartridges. Black color additive (MB Deltaplast USS7940 Black) was included in the injection molding.

3.2 Immunoassay measurements

This section explains how immunoassays were performed and how data was obtained and processed for analysis. Material tests were carried out to study how different materials work as a substrate for the immunoassay. In these tests cartridges were fabricated from different materials and immunoassays were performed on them. The Chamber 2 was used in material tests. The Effect of different geometries and micro structures on immunoassay was studied using the same material in all the cartridges. The last experiment studied how moving the sample during incubation affect immunoassay. In this experiment, reciprocating flow of the sample was used during incubation. In the all immunoassay experiments, the same protocol was used to prepare samples. Differences in incubation and washing protocols are described separately for each chamber type.

3.2.1 Sample preparation and assay steps

In the sample preparation, TSH in the TSA-BSA buffer (50 mM Tris-HCl, pH 7.75, 154 mM NaCl, 0.05% NaN_3 and 7.5% BSA) was diluted with DI-water to form concentrations 7.5 mU/l, 15 mU/l and 30 mU/l. Final samples were made from these by mixing 5 µl TSH solution with 30 µl Kaivogen buffer solution and adding 5µl nanoparticle solution to the sample. Final nanoparticle concentration in the sample was 10^8 particles in 40 µl. Nanoparticles were 107 nm polystyrene nanoparticles from Seradyn (Indianapolis, USA), which were doped with Europium(III)-chelates and coated with Anti-hTSH MAb-5409 at the Department of Biotechnology at the University of Turku, Finland. Zero-sample was made in the same way as the others but Kaivogen buffer was used instead of diluted TSH solution. In all experiments, three parallel samples were used for each sample concentration.

With chambers 1 and 2, immunoassay was performed in the following way. The sample was manually pipetted inside the chamber and cartridge was incubated in an oven (FD 53, BINDER GmbH) at 36 °C temperature. Immunoreaction was given 15 minutes to

occur and chamber was washed with 1 ml of 1×DELFIA® washing solution. Volume flow of 3.25 ml/min was used and washing was performed with the NE-4501 syringe pump (New Era Pump Systems, Inc., USA).

With the Chamber 3, 16 µl sample was injected inside the chamber and incubated 15 min. Wash included 133 µl washing solution which was pumped through the chamber with 433 µl/min flow rate. With these parameters, shear rate and washing time should correspond to those of the Chamber 2.

Reciprocating flow of the sample was used with the Chamber 4. 16 µl sample was injected inside the channel. The syringe pump was programmed to suck the sample over the reaction area and to move sample back and forth over the reaction area. 10 µl of the sample was moved 5 seconds in one direction and then in other. After 15 minutes, the sample was sucked out from the chamber area and washed with 100 µl of washing solution. A 100 µl/min flow rate was used to wash the Chamber 4.

3.2.2 Time resolved fluorescence measurement and data analysis

Time resolved fluorescence measurements were done with a well plate reader, Victor^2 Multilabel counter (Wallac/PerkinElmer). The measurement of a single spot was performed by measuring photon count during 400 µs time interval after 400 µs of the excitation. Excitation filter 340 nm and emission filter 615 nm were used. The multilabel counter gives measurement data as photon counts per second (CPS). A custom made clamp adapter was used to position the cartridge to a correct place on the fluorescence reader. The measurement protocol for the chambers 1 and 2 was programmed to scan over the chamber using 10x10 matrix (Figure 3.4). The diameter of the excitation point is approximately 1.8 mm and the separation between the excitation points is 1 mm. For the chambers 3 and 4 the measurement protocol was changed to scan 5x5 matrix as the reaction area is much smaller in these chambers.

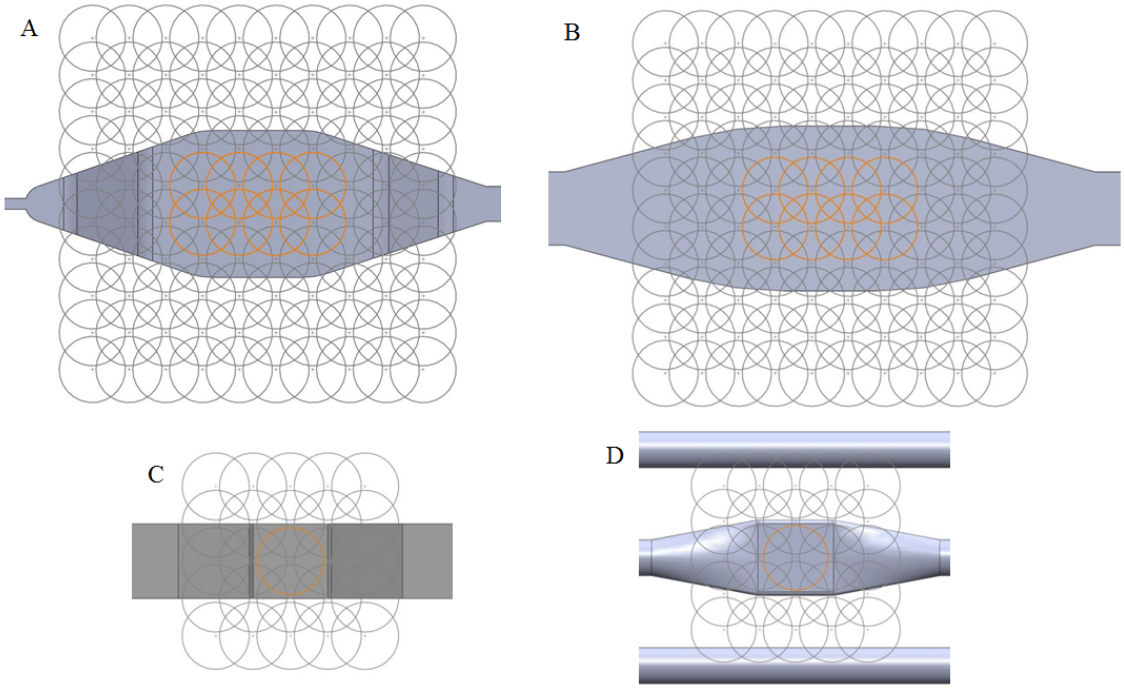

Figure 3.4. *Fluorescence measurement was done by scanning 10x10 matrix around A) the Chamber 1 and B) the Camber 2. 5x5 scanning matrix was used for C) the Chamber 3 and D) the Chamber 4. Orange circles represent measurement points which were used in analysis.*

Raw data from the multilabel counter was processed and analysed using Matlab®. The measurement data was obtained from measurement files and arranged to a matrix correspond the measurement protocol. The signal averages of 2x4 points from the center of the chamber were used in analysis for chambers 1 and 2 (Figure 3.4). These points were chosen as they are in the middle of the reaction chamber where points are fully inside the chamber area. For the thin chamber, measurement was done by scanning 5x5 matrix over the reaction area. Only the center point was used in the analysis as it was the only point fully inside the reaction area.

There was some displacement between individual cartridges even though the cartridge adapter was used. The matlab script was programmed to find the center of the chamber from the measured data in order to avoid taking wrong points to the analysis. Measurement points inside the chamber provide the highest signal values for the scan. The average signal value of the scan was used to find those points. The center of the chamber in the measurement matrix was calculated from those points and 2x4 matrix was positioned to the correct place.

Average of three parallel samples was calculated separately for every concentration and used to draw a concentration curve for immunoassay. In next step average background signal (signal of the zero sample, $\bar{s}_0$) was reduced from all values and linear regression line was fitted to data so that fitted line will intercept with the origin. Measurement

sensitivity was defined as the slope of this linear regression line and was calculated with least square method as:

$$Sensitivity = \frac{\sum_{k=1}^{Nc}(\bar{s}_{c_k} - \bar{s}_0)c_k}{\sum_{k=1}^{Nc} {c_k}^2} \quad (3.1)$$

Where Nc is a number of concentrations used in an immunoassay. c_k is a concentration value and $\bar{s}_{c_k}$ is a measured signal average corresponding the concentration. In most cases concentrations of samples were 0, 7.5, 15, 30 mU/L. Standard deviation of the background signal, σ_0, was calculated from zero sample values with equation:

$$\sigma_0 = \sqrt{\frac{1}{N}\sum_{i=1}^{N}\left(s_{0_i} - \bar{s}_0\right)^2} \quad (3.2)$$

Where N is an amount of parallel samples per concentration c and s_i is a measurement result of an individual sample. The standard deviations of the different concentration samples are indicating how reliably immunoassay is working over the whole measurement range. The standard deviation of the zero sample was used to calculate the limit of detection value for the assay with the Equation 2.23.

Percentage of covariance is parameter used to describe repeatability of immunoassays. This parameter is calculated as:

$$CV\% = \frac{\sigma_c}{\bar{s}_c} \times 100\% \quad (3.3)$$

Here, σ_c is a standard deviation and $\bar{s}_c$ is an average signal value of parallel samples of a concentration c. This parameter is used later in concentration curve plots as error bars.

3.3 FEM-modeling of immunoassay

A commercial FEM software COMSOL Multiphysics was used to develop 3D models for immunoassay reactions occurring inside the reaction chamber. The purpose was to study the effect of different geometries on the immunoassay and optimize the geometry for the cartridge.

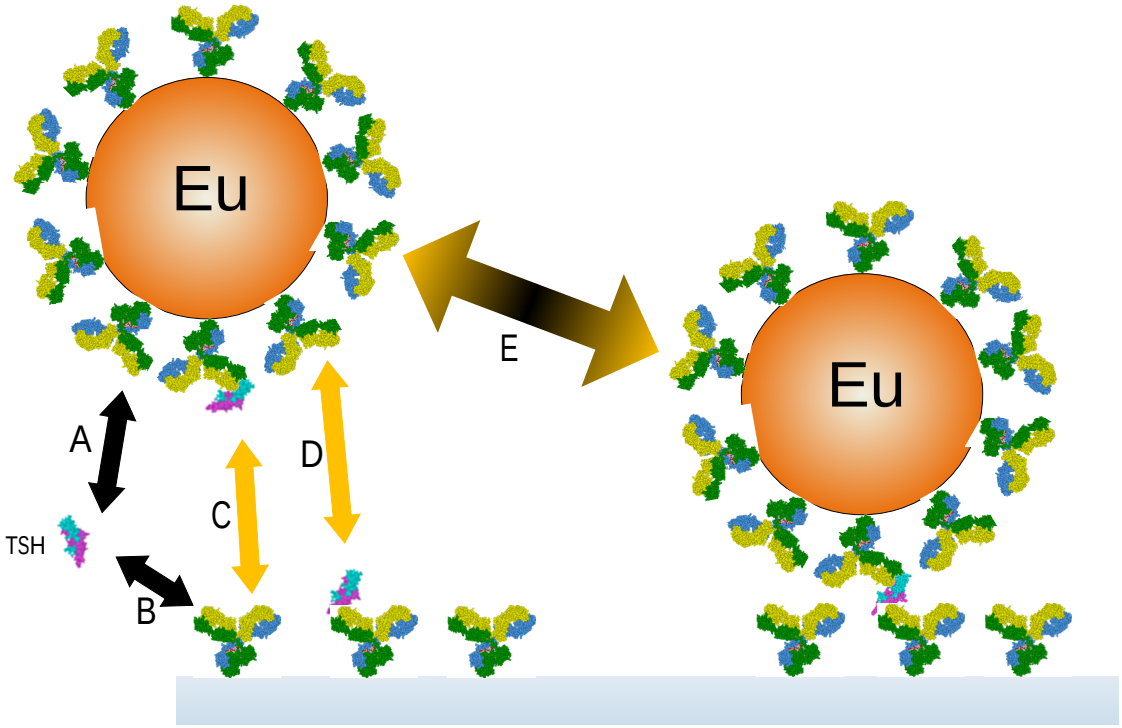

Figure 3.5. *Specific binding of the nanoparticle onto the surface. TSH molecule can bind A) to a nanoparticle or B) onto the surface. With help of TSH, the nanoparticle can bind to the surface C) through a TSH bound to the particle or D) through a TSH bound onto the surface. Overall, the nanoparticle binding on the surface is described with arrow E where all the reactions are combined. Modified with permission of Lasse Välimaa*

Immunoassay using nanoparticle labels contains complicated reactions (Figure 3.5). TSH molecules react not only with antibodies on the nanoparticle surface but also with the antibodies on the chamber surface. Through these bindings, a certain number of nanoparticles are able to bind to the surface with a certain reaction rate. Both the number of nanoparticles and the reaction rate depend on TSH concentration. Due to the lack of information about nanoparticles and the lack of software capabilities the models presented in this thesis are very simplified. Only the specific binding of the nanoparticles on the surface (Figure 3.5 E) is modeled. TSH binding reactions are left out. Next the different model cases are explained and the steps taken in model development are introduced.

3.3.1 Model cases

Immunoassay models are usually 2D models where the effect of walls is neglected. Thus, the Model 1 was a diffusion based model of the Chamber 1 (Figure 3.2 A) where the effect of the walls as the reacting surface was studied. Parameters affecting the reactions were studied with this model to see the effects. Model results were compared with experimental data and the most suitable parameters were used in the later models.

The Model 2 focused on the chamber height by using the geometry of the Chamber 2 (Figure 3.2 B). The height of the geometry was parametrized and different heights were compared. Hypothesis was that the chamber height does not have significant effect on a diffusion based immunoassay. Reason for this can be found the Equation 2.15. If a sample is incubated for 15 minutes, it means that a nanoparticle having a diameter of 107 nm is able to diffuse over a distance which is approximately 74 µm (Equations 2.14 and 2.15). If the chamber height is larger than this, a result should not change significantly. Only the particles from 74 µm distance have enough time to react with the surface. On the other hand, with lower height immunoassay run out of particles and thus signal level should decrease.

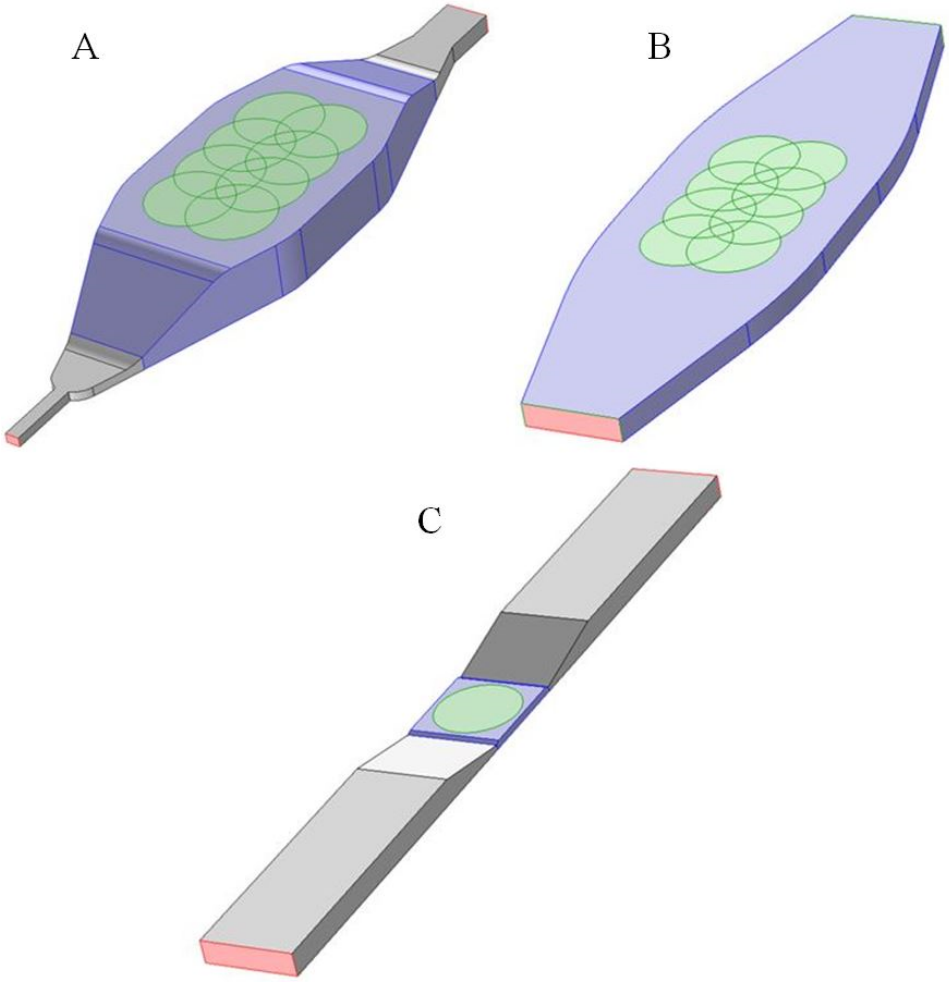

Figure 3.2. *Model boundary conditions on different geometries A) Chamber 1, B) Chamber 2 and C) Chamber 3. Green and blue areas are the reacting surface. Red ones are inlet and outlet for fluid flow. The surface concentration of bound nanoparticles on the green areas was calculated as a result.*

In the Model 3, fluid flow was added. The purpose was to study the reactions of the sample under a constant flow instead of a stationary incubation. Using a flowing sample, it is possible to increase the mass transfer to the surface and to help the system to reach equilibrium faster. The Model 3 used the Chamber 2 geometry and the

Chamber 3 was developed to maximize the mass transfer to a small reacting surface (Figure 3.2 C).

3.3.2 Modeling steps

A commercial CAD-software Solid Works was used to design geometries for mold fabrication. The same geometries were modified in such a way that only the necessary chamber geometry was imported to COMSOL. Model parameters and equations are described next. Used physics were "transport of diluted species", "surface reactions" and "laminar flow". [47]

Transport of diluted species physics

This physic set is used for modeling the mass transportation of small concentrations inside the reaction chamber. As the purpose was to model how nanoparticles bind on the surface, the model needed only one concentration to represent them. Equations describing mass transfer are:

$$\nabla \cdot (-D_i \nabla c_i) + \boldsymbol{v} \cdot \nabla c_i = R_i \tag{3.4}$$

$$\boldsymbol{N_i} = -D_i \nabla c_i + \boldsymbol{v} c_i \tag{3.5}$$

Here R_i stands for reaction rate and $\boldsymbol{N_i}$ is flux of specie i inside the system. c_i and D_i are the concentration and the diffusion coefficient of a substance i, respectively. $\boldsymbol{v}$ is the velocity field vector. [47]

Domain conditions used were "convection and diffusion" and "initial values". In first one D_i is defined by calculating value with equation 2.14. For nanoparticle which has a diameter of 107 nm, the diffusion coefficient is:

$$D_i = \frac{k_B \times 309.15\ K}{6\pi \times 7.0268 \times 10^{-4} Pa{\cdot}s \times 58.5\ nm} = 6.023 \times 10^{-8}\ \frac{cm^2}{s}$$

In the second domain the condition initial concentration of the nanoparticles is defined. As there is 10^8 nanoparticles in a sample of 40 µl concentration is then:

$$c_{NP} = \frac{10^8\ pcs}{N_A \times 40\ \mu l} = 4.151 \times 10^{-12}\ \frac{mol}{l} \tag{3.6}$$

N_A is the Avogadro number (6.022×10^{23} pcs mol^{-1}) which is used to transform the amount of substance to moles. Boundary conditions "no flux" and "flux" were used to describe walls and reacting surface. Flow based models included also "open boundary" boundary conditions for the inlet and the outlet.

"No flux" boundary was used in walls where there were no reactions occurring. Mathematically this boundary condition defines selected boundaries so that flux through the surface is zero:

$$-\boldsymbol{n} \cdot \boldsymbol{N_i} = 0 \tag{3.7}$$

$\boldsymbol{n}$ is the normal unit vector of the surface. "Flux" boundary condition was used to describe reaction rate R_i over the reacting surface. [47] Used reaction was simple monovalent binding reaction:

$$NP + BP \underset{k_d}{\overset{k_a}{\rightleftarrows}} NPS \tag{3.8}$$

Here NP indicates the nanoparticles in bulk solution, BP is binding places on the surface and NPS is the nanoparticles bound on the surface. The reaction rate for nanoparticles, R_{NP}, through the surface is:

$$R_{NP} = -\frac{d[NPs]}{dt} = -k_a[NP][BP] + k_d[NPS] \tag{3.9}$$

Square brackets mean the concentration of substance. The reaction rate is in this case negative as nanoparticles are reduced from bulk solution during the reaction. The number of the binding places and the initial concentration of the bound nanoparticles are defined in the "surface reactions" physics. Values for reaction rate constants were obtained from antibody data sheets. For antibodies on the surface (anti-TSH 5405) the values were 1.2×10^6 $M^{-1}s^{-1}$ and 1.9×10^{-4} s^{-1} for, respectively. For antibodies on the nanoparticles (anti-TSH 5409) the values for k_a and k_d were 2.1×10^6 $M^{-1}s^{-1}$ and 1.0×10^{-4} s^{-1}. Both values were tested, but the values of anti-TSH 5405 showed better correspondence to experimental data and were used in the rest of the models.

"Open boundary" boundary condition defines that all incoming flow has a specific concentration, $c_{0,i}$. On the other hand, if a flow is going out from the system, material just disappears from the boundary:

$$c_i = c_{0,i} \text{ if } \boldsymbol{n} \cdot \boldsymbol{v} < 0 \tag{3.10}$$

$$\nabla \cdot (-D_i \nabla c_i) = 0 \text{ if } \boldsymbol{n} \cdot \boldsymbol{v} \geq 0 \tag{3.11}$$

The velocity field $\boldsymbol{v}$ is neglected in the Models 1 and 2 as they are modeling stationary incubation. In flow based incubation model velocity field is first acquired by modeling fluid flow using "laminar flow" physics. [47]

Surface reactions

This physic set describes reactions occurring on surfaces. The set includes equations in reactions and mass transfer (flux $\boldsymbol{N}_{s,i}$) occurring on the surface. The reaction part includes both reactions occurring on between surface species $R_{s,i}$ and reactions between surface and bulk species, $R_{b,i}$. The number of surface species is also calculated as a fraction of filled binding places, θ_i. [47]

$$\frac{\partial c_{s,i}}{\partial t} + \nabla_t \cdot \left(-D_{s,i}\nabla_t c_{s,i}\right) = R_{s,i} \tag{3.12}$$

$$\boldsymbol{N}_{s,i} = -D_{s,i}\nabla_t c_{s,i} \tag{3.13}$$

$$\theta_i = \frac{c_{s,i}\delta_i}{\Gamma_s} \tag{3.14}$$

$$\frac{\partial c_{b,i}}{\partial t} = R_{b,i} \tag{3.15}$$

Here $c_{s,i}$ is the concentration of surface species, in this case bound nanoparticles. δ_i is the site occupancy number describing how many binding sites bound nanoparticle would cover. Γ_s is the number of binding places on the surface. $c_{b,i}$ is the concentration of nanoparticles in the bulk solution. [47]

It was assumed that particles are only able to bind on the surface and detach from it. It could be possible that particles are able to roll on the surface, but this kind of diffusion is very slow. Thus surface diffusion $D_{s,i}$ is assumed to be zero and the equations 3.12 and 3.13 are neglected.

Used boundary conditions were “surface properties”, “initial values” and “reactions”. “Reactions” boundary condition defines the reaction rate over the reacting surface the same way as in the transport of diluted species physics. In this case, the exception is that the reaction rate in equation 3.6 has an opposite sign. Nanoparticles are bound onto the surface and thus the number of bound nanoparticles is increasing.

“Surface properties” boundary condition defines the number of binding places on the surface as a binding place density (BPD). In a real situation, on the surface there are many antibodies near to each other. As the nanoparticle is much bigger than a single antibody the nanoparticle will cover more than one antibody as it binds. As there is no absolute information about the surface density of antibodies and about the coverage, simplification is done for the BPD parameter. Instead of using antibodies, the surface is

described as binding places for nanoparticles. One nanoparticle will in this case occupy only one binding place.

If nanoparticles form a triangularly closely-packed layer over the surface, they have a maximum density on the surface. For triangular closely packaged circles the coverage ratio is 0.9069. Therefore, for 107 nm diameter nanoparticles maximum BPD is:

$$BPD_{NP,max} = \frac{0.9069}{\pi r^2 \cdot N_A} = 1.6748 \cdot 10^{-10} [\frac{mol}{m^2}] \quad (3.16)$$

The site occupancy number was set to 1 as it was assumed that a bound nanoparticle covers only one binding place. Lastly the surface diffusion was set to zero and from "initial values" boundary condition, the initial concentration of bound nanoparticles was set to zero.

Laminar flow

Laminar flow physics is used to model a fluid flow inside the channels and chambers. The flow field, $\boldsymbol{v}$, was gained from the physic as a result. The result was coupled to "convection and diffusion" domain condition (Equations 3.4 and 3.5) inside the transport of diluted species physics. Equations used in laminar flow physics are based on the Navier-Stokes equation and for an incompressible fluid they are presented in Comsol as:

$$\rho \frac{\partial v}{\partial t} + \rho(\boldsymbol{v} \cdot \nabla)\boldsymbol{v} = \nabla \cdot [-p\boldsymbol{I} + \mu(\nabla \boldsymbol{v} + (\nabla \boldsymbol{v})^T)] + \boldsymbol{F} \quad (3.17)$$

$$\rho \nabla \cdot \boldsymbol{v} = 0 \quad (3.18)$$

$\boldsymbol{F}$ is a volume force caused by gravity. In these models it is neglected as volumes are very small and the gravitation does not have significant effect on the fluid flow. $\boldsymbol{I}$ is an identity matrix. [47]

Boundary conditions used in flow models are "wall", "inlet" and "outlet" boundaries. All walls were set to have a "no slip" condition, which means that the flow field on selected boundaries is zero:

$$\boldsymbol{v} = 0 \quad (3.19)$$

The outlet was set to have "pressure, no viscous stress" condition so that the pressure, p, in the outlet was zero and viscous forces are vanishing at the boundary:

$$p = p_0, [\mu(\nabla \boldsymbol{v} + (\nabla \boldsymbol{v})^T)]\boldsymbol{n} = 0 \quad (3.20)$$

The inlet was set to have the “laminar inflow” condition with a certain flow rate V_0:

$$L_{entr}\nabla_t \cdot [-p\boldsymbol{I} + \mu(\nabla \boldsymbol{v} + (\nabla \boldsymbol{v})^T)] = -p_{entr}\boldsymbol{n}, \nabla_t \cdot \boldsymbol{v} = 0 \quad (3.21)$$

Entrance length L_{entr} is used to model a channel which has the length of L_{entr} and cross-section the same as the inlet does. From this solution the initial velocity field and entrance pressure, p_{entr}, are calculated for the model. Default value of 1 m was used in the boundary condition as it should be long enough for the model to reach a laminar flow field. In flow based incubation models, 40 µl per 15 minute flow rate was used as it corresponds the sample volume and the incubation time. In reality, achieving this low flow rate is challenging with the syringe pump. Therefore flow based models are done to illustrate the effect of the flow on the immunoassay. [47]

4 RESULTS AND DISCUSSION

In this chapter all the results from the experiments are presented and discussed. Section 4.1 discusses results from simulated models. Section 4.2 includes results from empirical experiments focusing on material and geometry comparisons.

4.1 Immunoassay models

In this section the results of different models are presented. Model 1 simulated the Chamber 1 and was used to study how different model parameters affect the surface concentration of the sample. Model 2 studied how the chamber height affects immunoassay. Model 3 studied the effect of a fluid flow on immunoassay.

4.1.1 Evaluation of the immunoassay model

The diffusion based model of the Chamber 1 was compared with data which contained a five-day incubation results obtained from the NanoFlow project. All curves were normalized to have the maximum value 1, because correlation between nanoparticle surface concentration and the amount of fluorescence is not known. As seen from Figure 4.1 a simulated curve is correlating quite well with the real experiments. The reaction rate constants of antibody 5405 seem to give a better fit for experimental data. Probably because TSH molecules are better attached to antibody 5409 and thus the slower antibody is limiting the binding reaction.

As the nanoparticle may have a different reaction rate constants compared with a single antibody [37] simulation was driven using different k_a and k_d parameters (Equation 3.6). This was done to get a better fit for the concentration curve and to get better understanding of the system's behavior. Parameters used were 1, 2, 3 and 5 multipliers for k_a and the same values as dividers for k_d. The second parameter studied was the number of binding places on the surface. Multipliers used for the binding place density were 0.8, 0.6, 0.4, 0.2 and 0.1. The effect of the reaction rate to the immunoassay is presented in Figure 4.2 and the effect of the binding place density in Figure 4.3.

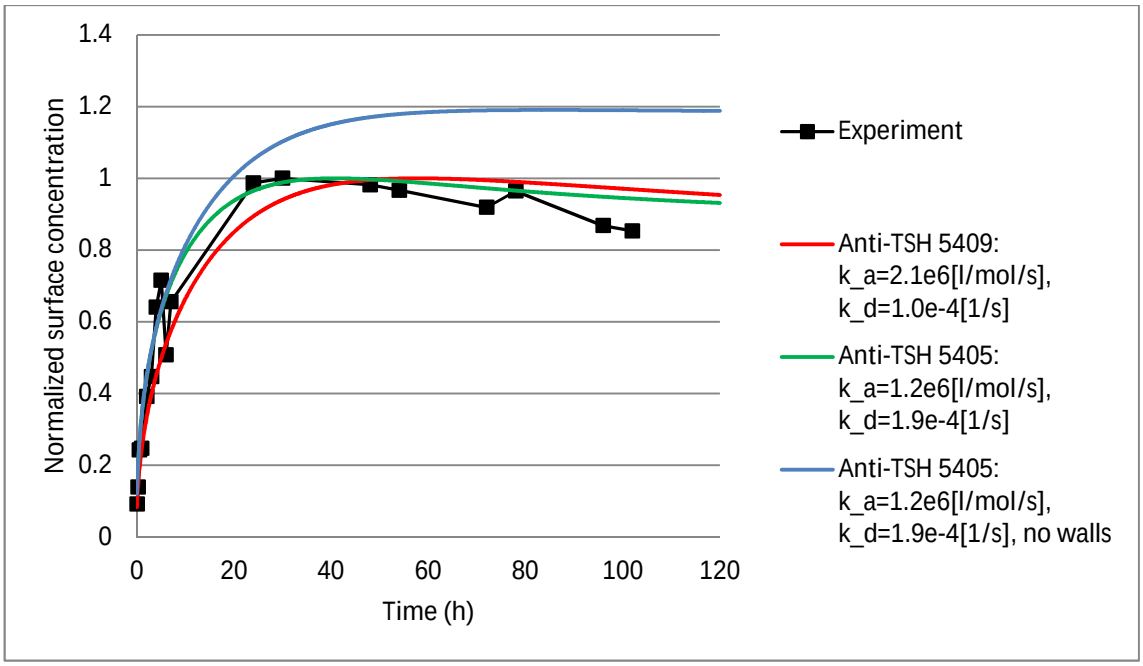

Figure 4.1. *Simulation results of the Model 1 compared with the five-day experiments.*

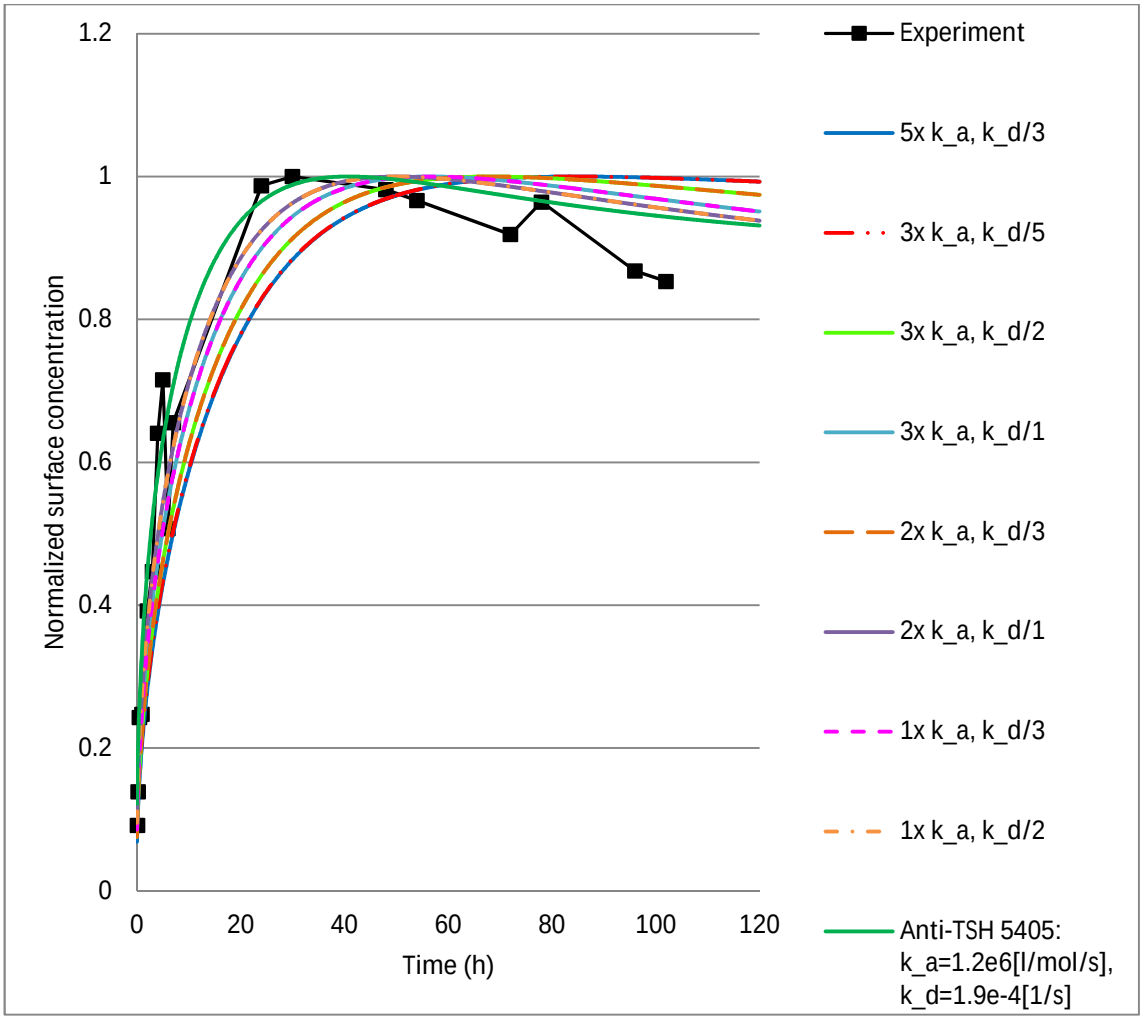

Figure 4.2. *The Model 1 results: The effect of different reaction rate constants on the surface concentration.*

It was noticed that the model gave identical results for those k_a and k_d values which had the same proportion k_a/k_d. When proportion increases the peak of the maximum concentration shifts to a later time point and vice versa. As data is normalized it should be mentioned that as the k_a/k_d ratio increases also the concentration of bound nanoparticles increases.

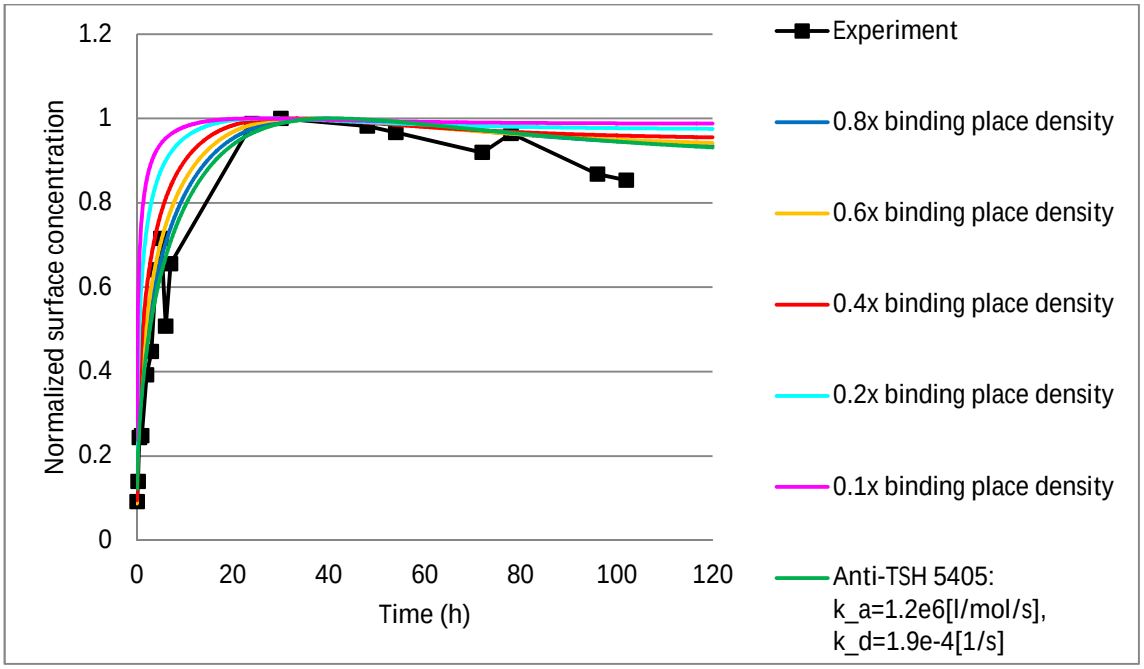

Figure 4.3. *The Model 1 results: The effect of the binding place density on the surface concentration.*

With a lower binding place density value the peak shifts to an earlier time point. In the end, there was no clear decrease on the scaled surface concentration. Reason for this might be the fact that when there is a small amount of binding places, the surface is saturated faster than with a higher binding place amount. Thus the maximum signal value is also reached faster. On the other hand as the surface gets saturated particles are able to spread faster into corners. Therefore the signal does not drop after the maximum surface concentration as much as with the higher BPD. One has to remember that the curves are scaled and in the real case a surface with less binding places would also produce less signal than a surface with a higher BPD. Because later models are used to simulate only 2 h incubation, it seemed reasonable to use the original values of anti-TSH 5405 antibody which gave the best fit for experimental results within 10 h.

As mentioned earlier with diffusion models it is important to take into account the effect of the walls. When comparing simulations where walls are neglected to simulations where they are included as reacting surface the difference is quite significant (Figure 4.1). Reason for the difference is a concentration gradient which is formed perpendicular to all reacting surfaces (Figure 4.4). When walls act as a reacting surface,

mass transfer to corners is decreased. Bindings occur first to middle parts of the walls and the bottom. As nanoparticles may detach from the surface they will slowly spread towards the corners. This is the most probable reason for the signal to lower after 10 h incubation. In the end reactions reach equilibrium everywhere and surface concentration reaches the same value also in the corners. The whole system is in equilibrium and thus concentration all around the chamber reaches constant value.

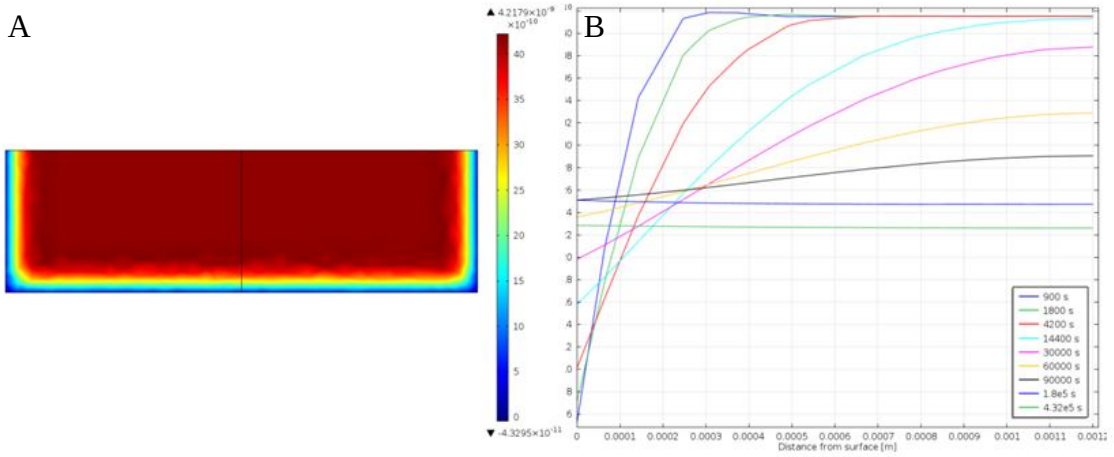

Figure 4.4. *A) Cross-section of the Chamber 1 from time point 15 min shows that a concentration gradient is formed in the U-shape along the walls. B) Concentration measured along the centerline of the chamber shows the spreading of the diffusion layer during the incubation.*

Without walls, a concentration gradient is formed only to the bottom. Thus also corners nearly get the same amount of particles as the center part of the bottom. From these results, it would be reasonable to assume that walls are disturbing the process to reach equilibrium. To take into account this an optimal reaction chamber should be as flat as possible in order to minimize the effect of the walls.

4.1.2 Chamber height studies

The geometry of the Chamber 2 was used to study the effect of the chamber height. The Model 2 was the same as the Model 1 but instead of using the Chamber 1 the Chamber 2 was used. As the Chamber 2 was flat, it was more suitable to parameterize the chamber height. Results of the simulations can be seen in Figure 4.5.

When the chamber height decreases the maximum number of particles on the surface will also decrease. This is caused by a limited sample volume inside the chamber. The number of nanoparticles is simply running out with a lower chamber, because of the increasing surface to volume ratio. It was estimated that during 15 minutes a nanoparticle is able to diffuse over 74 µm distance at the maximum. This seems to be correlating quite well with the model as 75 µm high chamber reaches equilibrium already after 30 minutes. The reason for the longer time might be that the diffusion layer

is increasing all the time and the concentration gradient is getting lower. As the model uses gradients to calculate fluxes it means that the flux through the chamber is decreasing over the time. An analytical model (Equation 2.14) does not take this in to account and thus the model result differs from it.

From Figure 4.5, one can see that curve starting points differ from each other. This is caused by numerical errors during simulations. This is the most probably caused by rounding errors as concentration values are so small. This happens in all the cases but it does not affect results significantly.

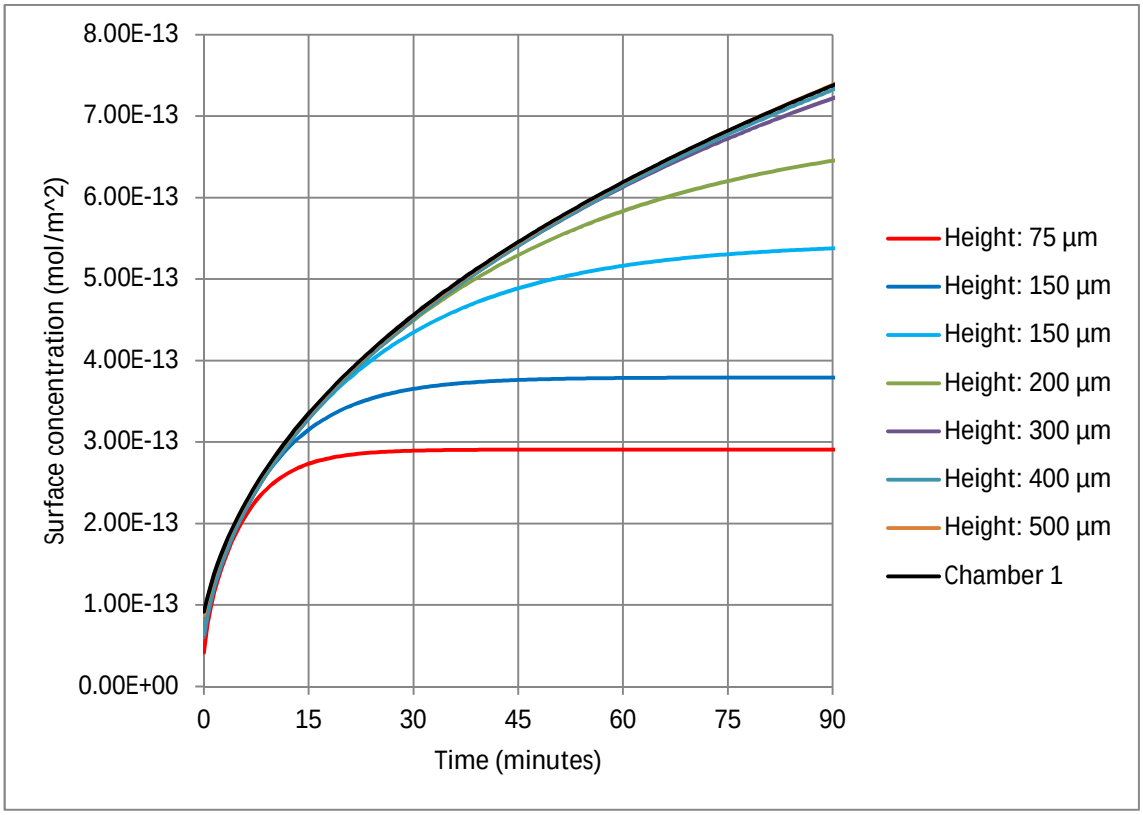

Figure 4.5. *The Model 2 results. The Chamber 2 geometry was used with different heights. The result from the Chamber 1 is shown as a reference.*

15 minute incubation time was used in experiments. According to these simulation results 150-200 µm height would be the best for the chamber. A smaller chamber will run out of nanoparticles and thus have lower signal values. On the other hand a chamber higher than 200 µm will have some extra sample volume which is never used in the reaction.

4.1.3 Flow based incubation studies

The purpose of a flowing sample was to prevent the formation of the concentration gradient and especially to prevent the gradient from spreading and thus to decrease the mass transfer towards the surface. When there is a flow through a chamber new

particles are coming over the surface all the time and thus more bindings will occur. This was simulated by using the same geometries as in the second model but coupling the fluid flow to the Model 3. From the results (Figure 4.6) it is clearly seen that with a constant flow rate binding is related to the chamber height. As the chamber height gets lower the flow velocity gets higher. The higher the flow velocity is thinner the diffusion layer gets and providing higher mass transfer. This means that reactions occur faster.

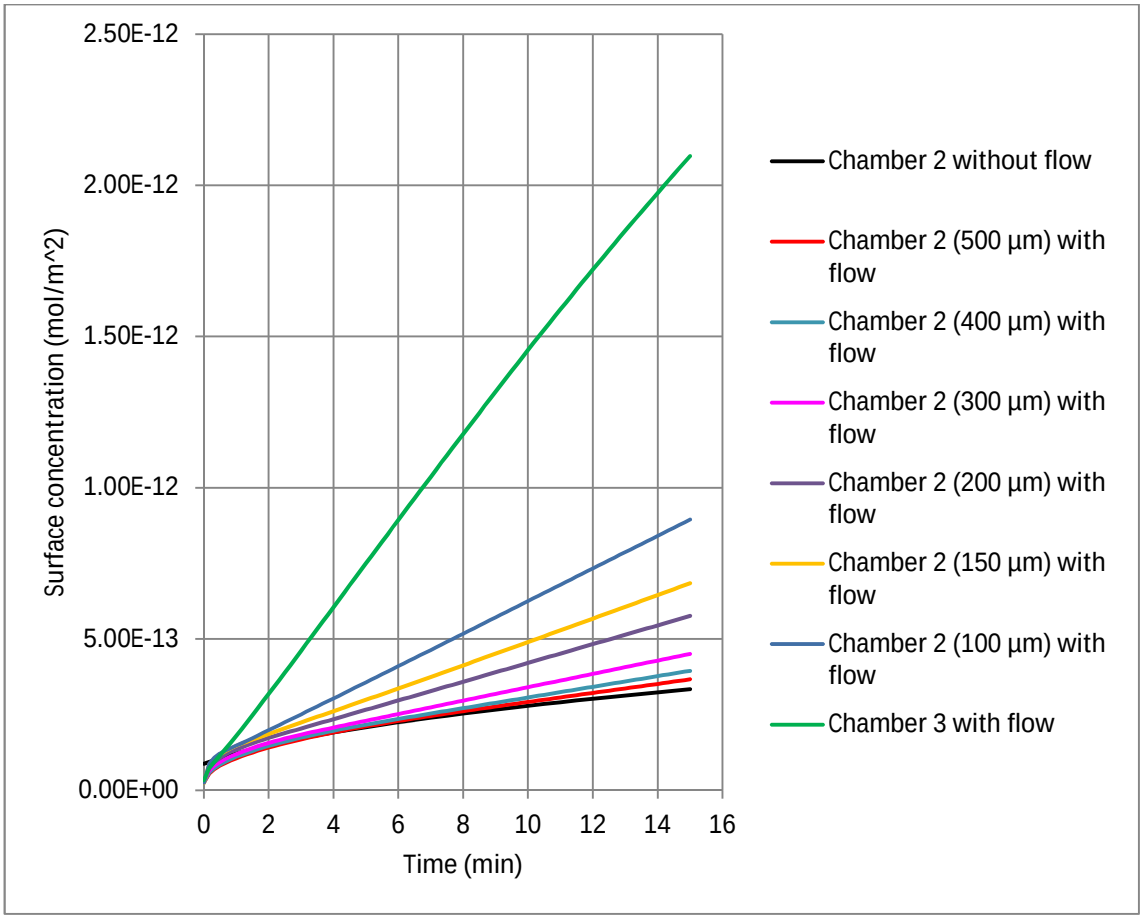

Figure 4.6. *The Model 3 results. When a flow is applied to the immunoassay, the surface concentration is increasing as the chamber height is decreasing. Height is marked inside parentheses. Flow rate 40 µl in 15 min was used in the model.*

After these simulations it was clear that there would be no sense to have a diffusion limited system. The Chamber 3 geometry was designed so that the reaction area would be as small as possible. The bottom was decreased to a rectangular area of 2x2 mm. Reason for this was that Victor multi-label counter had an excitation spot which is an approximately circular area with a diameter of 1.8 mm. Theoretically, measurement could be conducted using a single measurement point without scanning a large area around the chamber. The height of the chamber was 150 µm as it was still providing enough particles to make wet lab experiments using stationary and flowing sample incubations for a comparison. One reason for choosing this height was also the fact that producing smaller features using injection molding would be challenging.

4.2 Immunoassay experiments

This section describes the results of immunoassay experiments. In Section 4.2.1 results of the material experiments using the Chamber 2 are presented. The purpose was to study the effect of the material on the immunoassay performance and find the most suitable material for the cartridge. Section 4.2.2 presents the results of the geometry comparison between chambers 1 and 2. Section 4.2.3 presents the immunoassay results of the Chamber 3. The effect of the micro structures on the immunoassay is also presented in this section. The last section 4.2.4 presents results of the Chamber 4 where the immunoassay was performed using a reciprocating flow.

4.2.1 Different polystyrene grades

The immunoassay performance on different polystyrene grades and PMMA was studied using the Chamber 2. Results of the experiments are presented in Figure 4.7 and Figure 4.8. In Figure 4.7, different plastic grades are presented with their own color. In the legend, the material of injection molded channels is written before a slash and the material of the cover plate is written after the slash.

From the signal averages it is clearly seen that polystyrene grade Empera 124N was giving the highest signal levels. The difference between PS 158K and Styrolux was not significant. PMMA gave the lowest signal values. PMMA probably has a poor transmittance for the excitation wavelength.

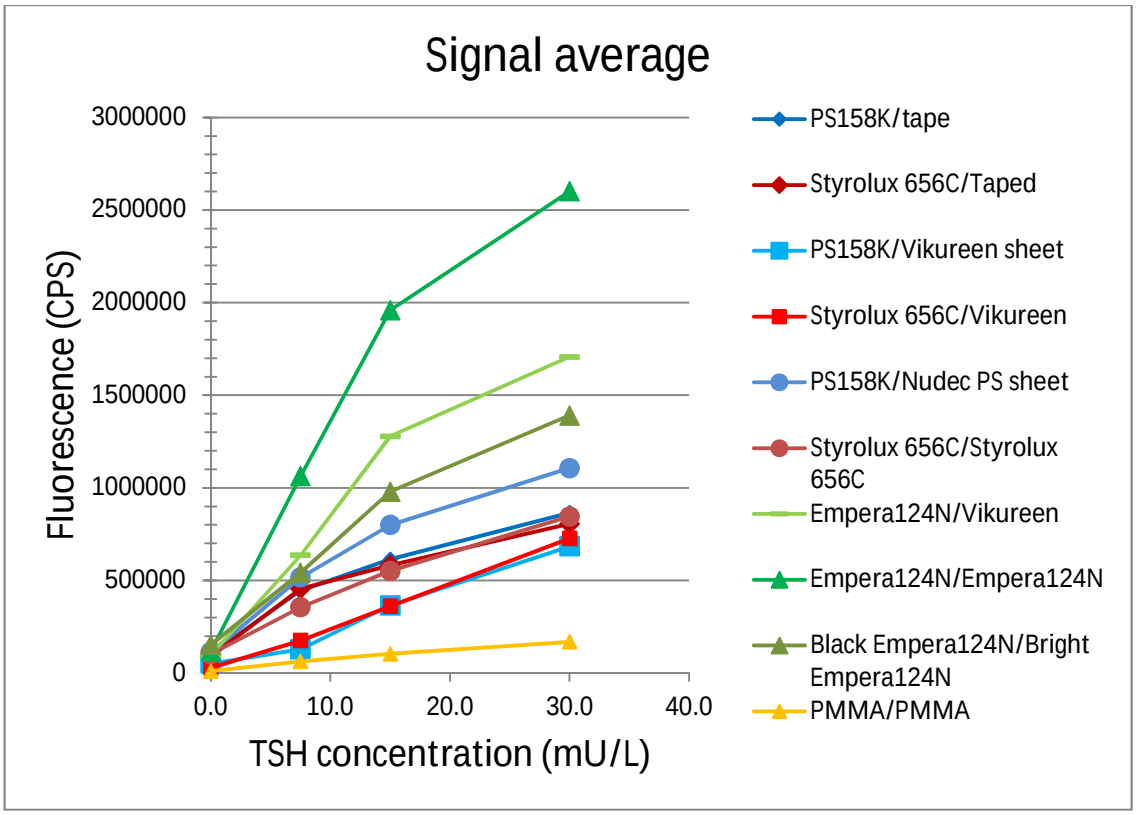

Figure 4.7. *Results of the material experiments. Average of three parallel samples was used.*

Figure 4.8 presents a background signal level average (Bgr), standard deviation of the background signal (Bgr-σ, Equation 3.2), measurement sensitivity (Equation 3.1) and the limit of detection (Equation 2.23) for each experiment. The results are scaled in y-axis to fit in the figure. Scaling of the value is informed after the unit in the x-axis. Examination of this figure reveals that there was no significant difference in the background levels between the polystyrene grades. A comparison test gave very low background values for both PS 158K and Styrolux grade, but the reason for this was not tracked down. Background levels are affected by the coating and its properties to prevent unspecific binding. Also the concentration of nanoparticles affect as there would be more particles to bind on surface as their concentration increases. Because all the samples are done similarly there might have been some problem with the coating and the surface might have had less antibodies.

Deviations of background signals are in most cases lower with laser welded cartridges. Channel cross-section varies with taped cartridges as taping is done manually. This may explain larger deviation for those cartridges. Also the tape material may have some negative effect on deviations. For Empera, there was also a high deviation value in one experiment. This can be explained by problems with bubbles during the washing step.

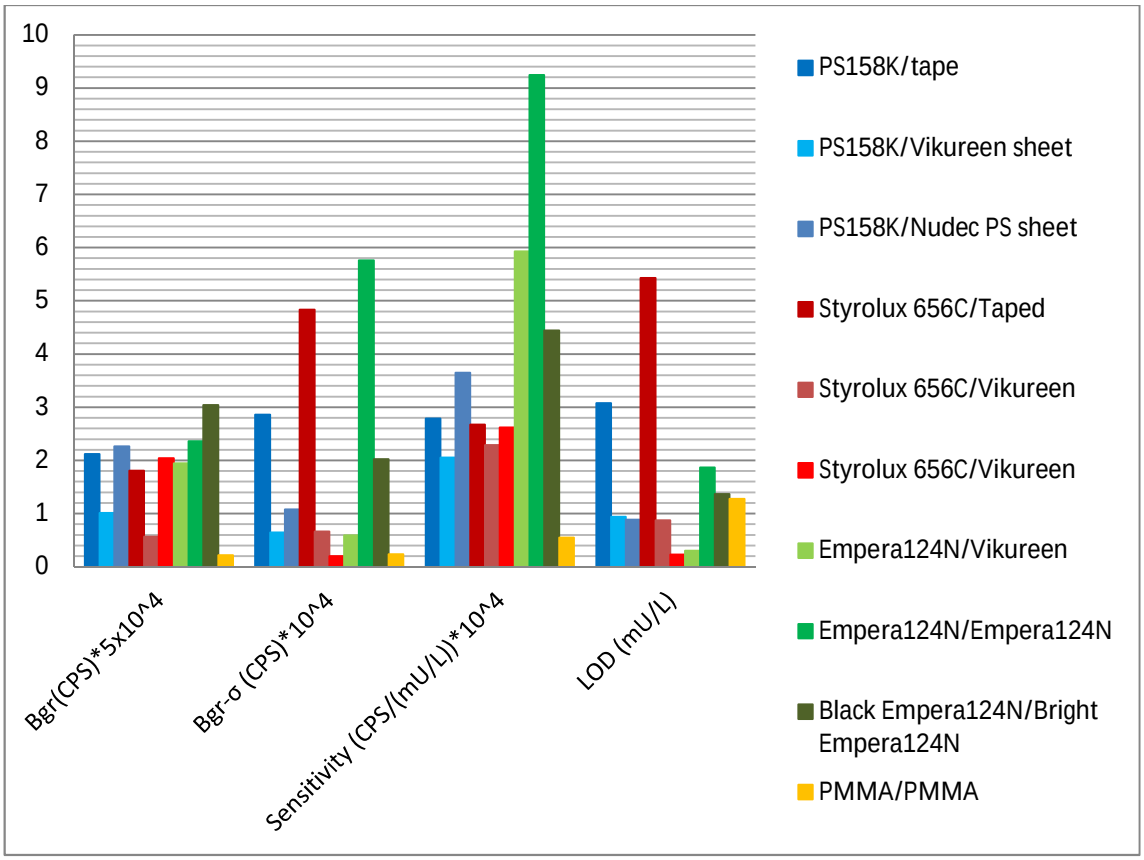

Figure 4.8. *Background, background deviation, sensitivity and limit of detection values of the material tests. Units and scaling of the data is shown on X-axis.*

The Figure 4.8 does not have space for the error bars. As zero samples had lowest average signal values, their percentages of covariance were mostly around 20%. For other samples these values were around 14%.

As background values are nearly on the same level in each polystyrene case, it is quite obvious that sensitivity is the best with those materials which also has a high signal level. Sensitivities of Empera were 92.4×10^3, 59.3×10^3 and 44.4×10^3 CPS mU^{-1} L^{-1} as other grades reached a maximum of 36.5×10^3 CPS mU^{-1} L^{-1}.

Limit of detection values are in most cases around 1 mU/L. For taped cartridges and one Empera batch, LOD values are much higher due to high background deviation. The best LOD result, 0.23 mU/L, was obtained with Styrolux 656C, but in that experiment the background deviation was exceptionally low, only 2030 CPS. If the deviation would have been on the same scale with the others, the LOD would not differ very much. On the contrary as the deviation of Empera is around the same level with the others or more, it is more probable that it actually has the best LOD value, 0.30 mU/L.

Although Empera seemed to be the best material for the immunoassay there were problems in producing intact cartridges from it by injection molding. The same problem occurred with PS 158K grade. These two were very brittle plastics and thus they tended

to crack when ejected from the mold. The rest of the experiments were carried on with Styrolux 656C grade as it was a more durable material for injection molding.

4.2.2 Reaction chamber geometry

Comparison of reaction chambers 1 and 2 were carried on with cartridges made of Styrolux 656C. Experiments were done separately and thus the tests done using the Chamber 1 miss the results having a concentration 7.5 mU/L. When comparing the results in Figure 4.9 it can be seen that the concentration curves are quite similar and there are only slight differences in signal levels. As nanoparticles are able to diffuse 74 µm distance during incubation the whole chamber volume is not exploited. Only a small number of particles are able to react with the surface in both geometries and thus the concentration curves are so similar.

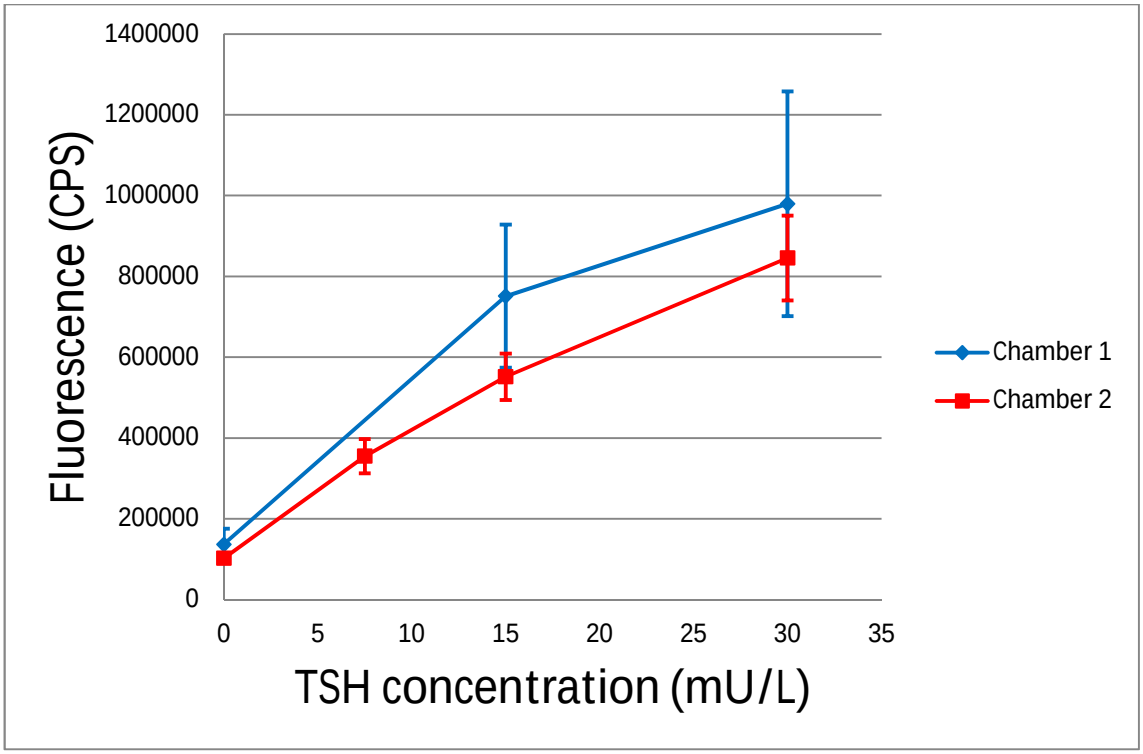

Figure 4.9. *Concentration curves of immunoassays done in chambers 1 and 2.*

The background level was slightly smaller in the Chamber 2, 102×10^3 CPS, compared with the Chamber 1, 137×10^3 CPS (Figure 4.10). Background deviations were not comparable as the results for the Chamber 2 were the same as those which had exceptional low values in the material comparison. The background deviation of the Chamber 1 was 38.7×10^3 CPS and as for the Chamber 2 it was 2.0×10^3 CPS. This result indicates that the number of the parallel samples should have been much larger than three.

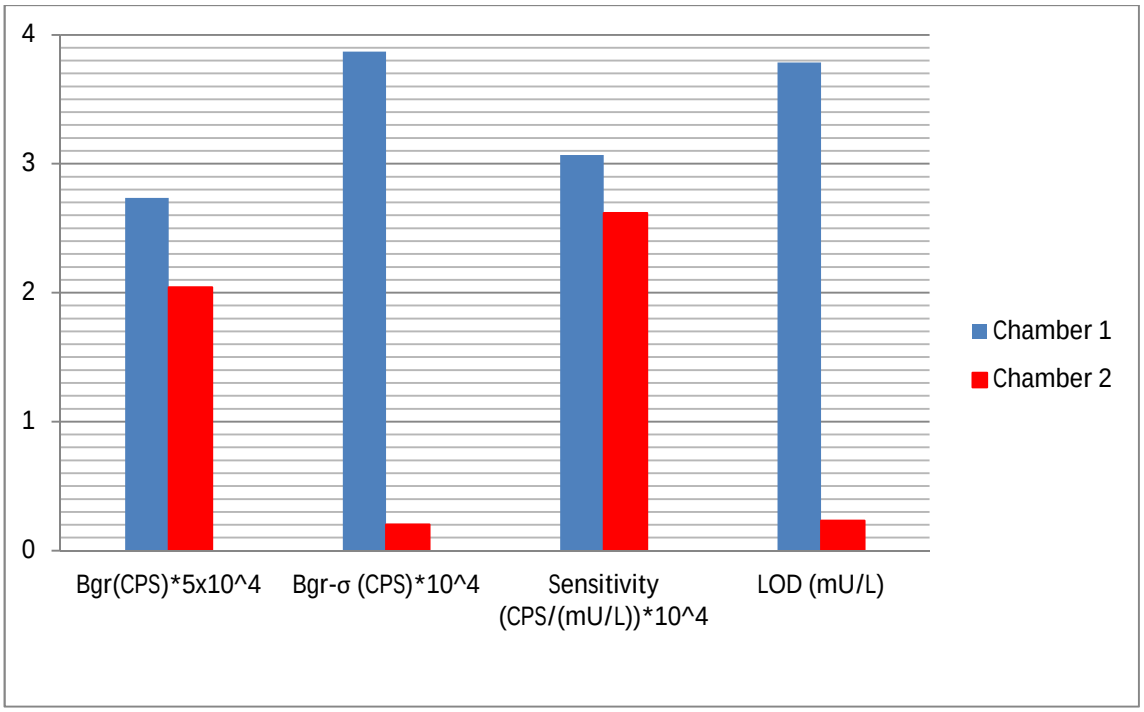

Figure 4.10. *Background levels, background deviation, sensitivity and limit of detection values of the chambers 1 and 2.*

Sensitivities were 30.7×10^3 CPS mU^{-1} L^{-1} for the Chamber 1 and 26.2×10^3 CPS mU^{-1} L^{-1} for the Chamber 2. LOD values were 3.79 mU/L for the Chamber 1 and 0.23 mU/L for the Chamber 2. One reason why the Chamber 1's deviation values are high is that washing is less effective than in the Chamber 2's case. As for the Chamber 2, washing solution go through the chamber in more laminar manner compared with the Chamber 1. The Chamber 1 inlets are very small and they are not at the same level as the reacting surface. As the chamber has a cup like structure it is possible that most of the washing solution is just flowing through the chamber without flushing the surface properly. Another problem is the large difference in size between the chamber and the inlet channel which may in some cases cause bubbles inside the chamber when the sample is sucked out. These bubbles will definitely disturb proper washing and cause the higher standard deviation for the zero sample.

4.2.3 Immunoassay on microstructures

The nanoparticle batch was changed before doing the experiments using the Chamber 3 geometry. Thus the results given by this geometry are not fully comparable with those of the earlier geometries.

The effect of the surface roughness was studied using the Chamber 3 geometry where two of the channels had different laser ablated surfaces. One chamber had an array of single hemispherical structures (Figure 4.11 A and C) and other chamber had an array of four hemispherical structures grouped together (Figure 4.11 B and D). The third

surface was a smooth polished surface which was used as a reference. Holes in the mold were 5 µm deep, but replicated structures were only 2.6 µm high. As plastic was transparent it was not possible to measure the surface roughness with an optical profilometer. Although replication was not perfect it was decided to test immunoassay on these surfaces. From profilometer pictures it was assumed that the surface consisting of the grouped structures would have a larger total area and thus it should give higher signal values.

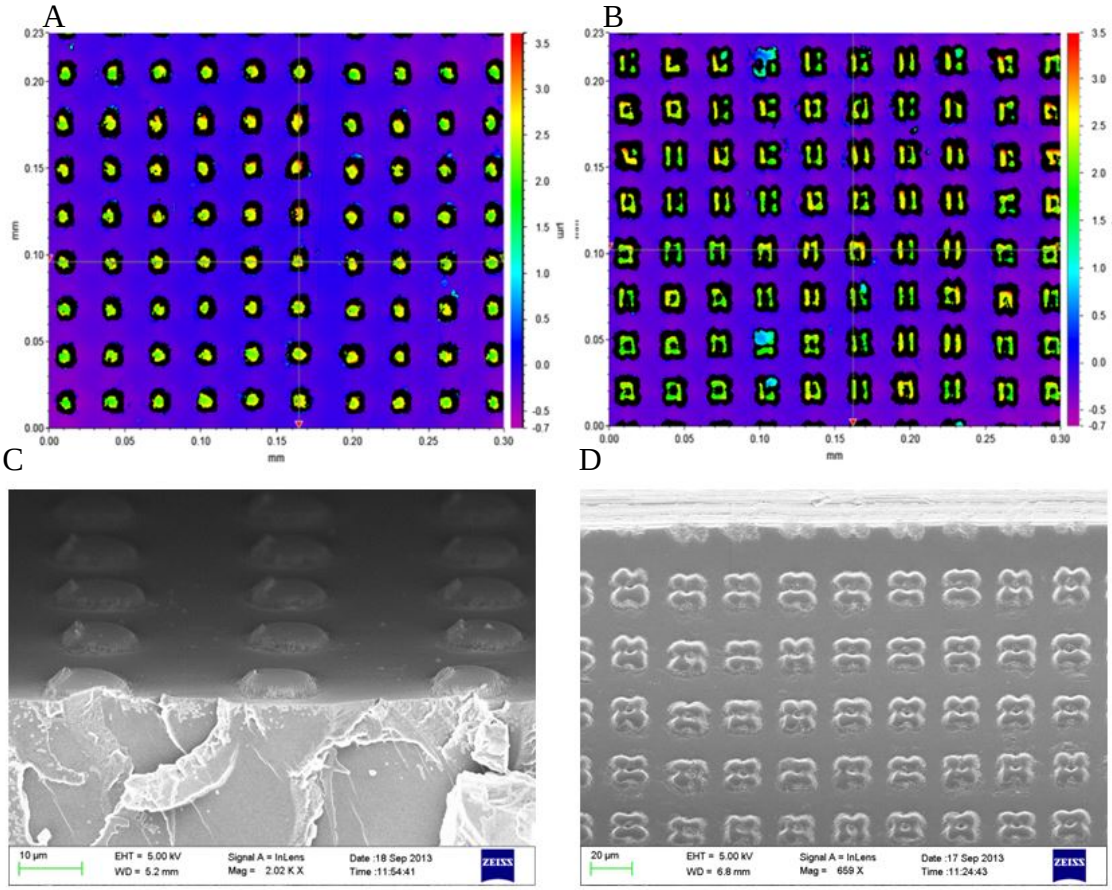

Figure 4.11. *Profilometer and SEM pictures of the micro structured surfaces. A and C: Array of single structures and B and D: the array of lumped structures. SEM pictures are courtesy of Jarkko Mutanen.*

Figure 4.12 shows that both micro structured surfaces gave higher signal values compared with the smooth polished one. Surprisingly, the single structured surface gave much higher signal values compared with the grouped structures. Sensitivities were 2.91×10^{3} CPS mU^{-1} L^{-1}, 5.08×10^{3} CPS mU^{-1} L^{-1} and 10.94×10^{3} CPS mU^{-1} L^{-1} for smooth, grouped structures and single structures, respectively.

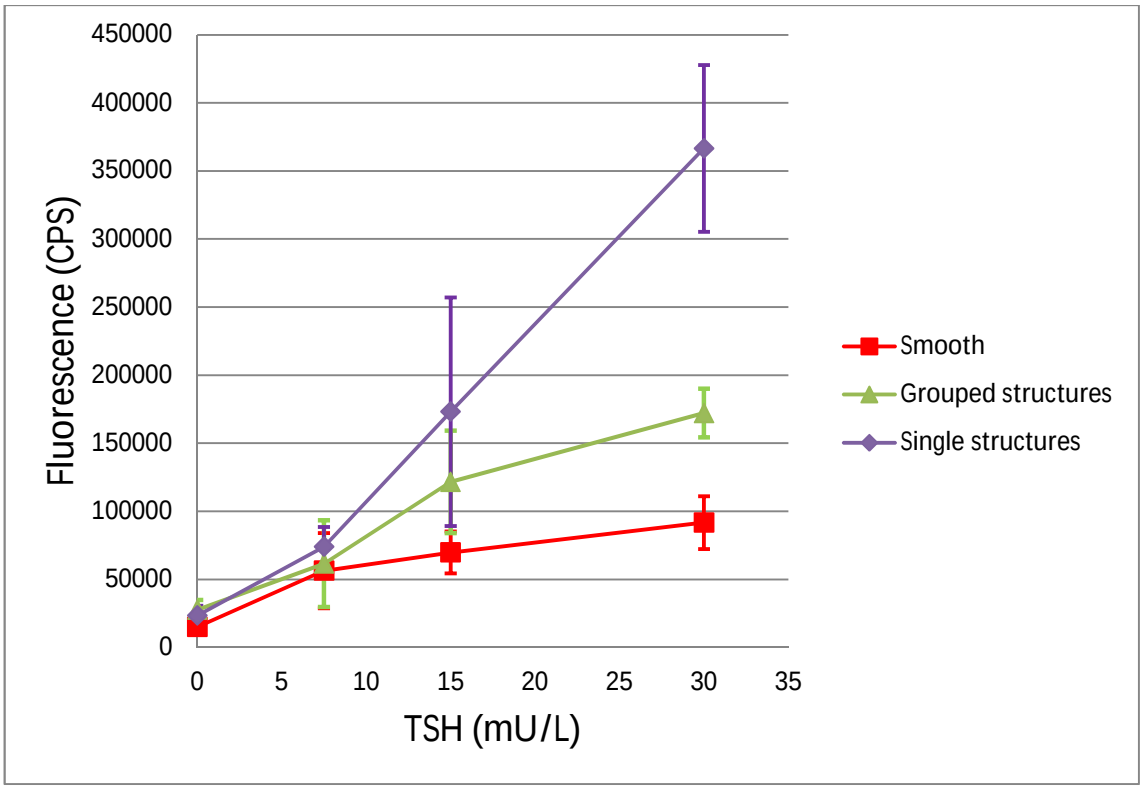

Figure 4.12. *Signal average plots of thin chamber experiments show that micro structures have a significant effect on immunoassay results.*

Unfortunately, as the surface area is increases it seems that the possibility for unspecific binding increases as well. This can be seen from the background levels which were clearly higher for the chambers containing microstructures compared with the chamber which did not. Background values were 14.9×10^3 CPS, 27.7×10^3 CPS, 23.5×10^3 CPS for smooth, grouped structures and single structures, respectively.

Figure 4.13 shows that standard deviations of background averages were also higher with micro structured surfaces. Values were 2.7×10^3 CPS, 7.2×10^3 CPS, 7.1×10^3 CPS for smooth, grouped structures and single structures, respectively. Limit of detection values were 2.78 mU/L, 4.27 mU/L and 1.95 mU/L for smooth, grouped structures and single structures, respectively.

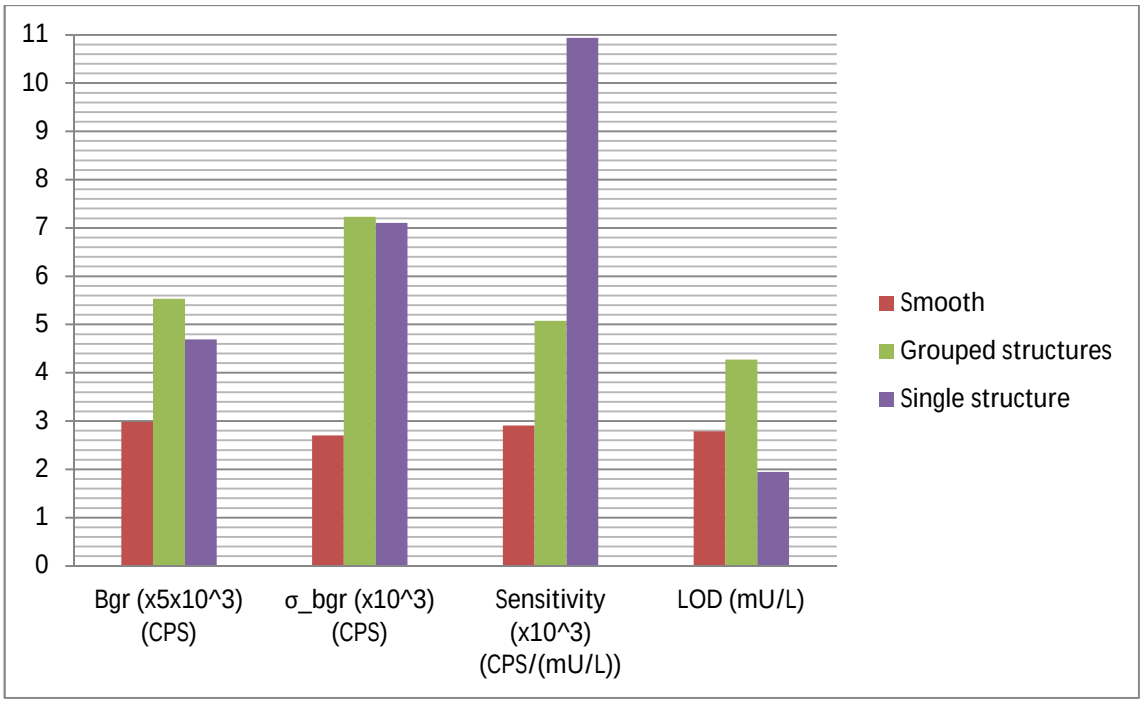

Figure 4.13. *Background levels, background deviation, sensitivity and limit of detection of the Chamber 3.*

Low signal values of the Chamber 3 compared with the chambers 1 and 2 can be explained with the new nanoparticle batch which was known to have a lower label amount than the earlier batch. Assuming that there was the same number of nanoparticles on the polished surface of the Chamber 3 as there was in the Chamber 1, it would be possible to use scaling to compare the results. Background level was 14.9×10^3 CPS for the smooth chamber and 137×10^3 CPS for the Chamber 1. The Chamber 1 has nearly a tenfold higher background level. If sensitivities, 2.91×10^3 CPS mU^{-1} L^{-1} for the Chamber 3 and 30.7×10^3 CPS mU^{-1} L^{-1} for the Chamber 1, are compared they seem to be quite similar with tenfold scaling.

The main problem with the Chamber 3 was the capillary effect which caused bubbles to occur inside the chamber during washing. These bubbles prevented proper washing and thus background deviations were high. This again caused large limit of detection values. Because of these problems the Chamber 4 geometry was designed and reciprocating flow during sample incubation was tested with it.

4.2.4 Immunoassay using reciprocating flow

In the last experiment, the sample was moved over the reaction area in the Chamber 4. This was compared with the Chamber 2 where the sample was incubated stationary. There were quite many problems. The laser welding of these chambers failed and thus the test was carried on using cartridges which were taped with adhesive tape. Failure of the welding might have been caused by a small scratch in the mold which prevented a proper contact with the cover plate. This caused a poor welding seam which leaked. The

second reason could be that the material was changed. Styrolux 656C was out of stock and thus KR-01 (from K-resin), which should be similar material was used in this experiment. KR-01 probably has slightly different melting properties and was thus welded poorly.

There were also some technical problems with the syringe pump and connections with cartridge inlets during reciprocating incubation and thus the data from the concentration 15 mU/L was lost. In the rest of the moving experiments, it was noted that fluid did not move as it was supposed to. The pump was programmed to move 10 µl volume of the sample back and forth, but the movement was much less in all cases.

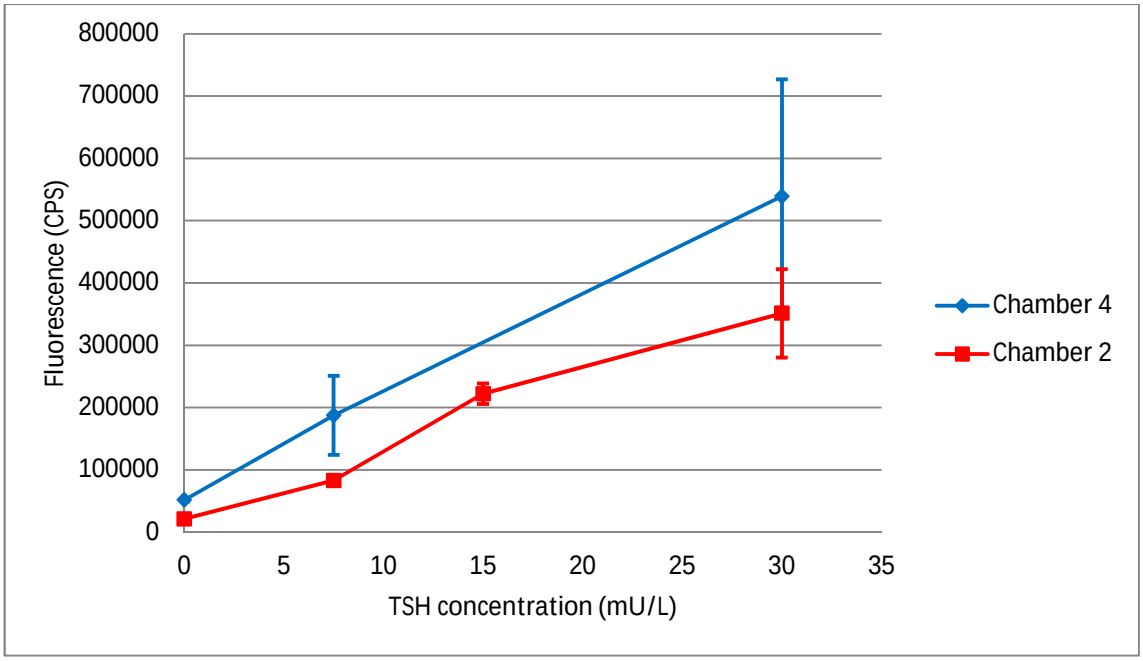

Figure 4.14. *Signal averages from the Chamber 4 with reciprocating flow of the sample compared with stationary incubation in the Chamber 2.*

Even though the experiment was not perfect, it showed that the Chamber 4 having a reciprocating flow gave higher signal values than the Chamber 2 where the sample was incubated stationary (Figure 4.14). It was assumed that as there are more particles coming towards the surface when the sample is moving the number of bound nanoparticles increases. Thus sensitivity should increase too as it seems to happen. Sensitivities were 16.4×10^3 CPS mU^{-1} L^{-1} and 11.3×10^3 CPS mU^{-1} L^{-1} for the Chamber 4 and the Chamber 2, respectively.

The background level is over two times higher with reciprocating movement, 51.8×10^3 CPS, compared with stationary incubation, 21.1×10^3 CPS (Figure 4.15). It may be possible that as the flow is increases the specific binding it also increases the unspecific binding.

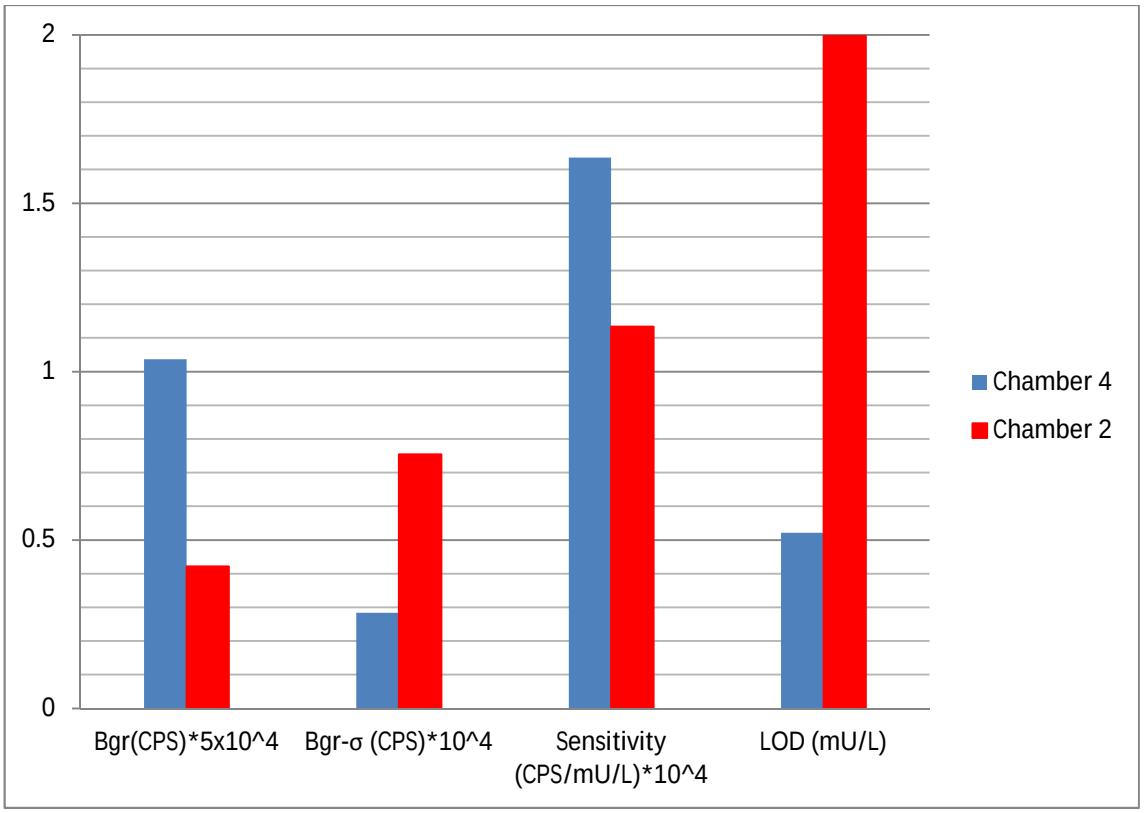

Figure 4.15. *Background levels, background deviation, sensitivity and limit of detection of comparison of the stationary and the reciprocating incubation experiment.*

Limit of detection values were 1.99 mU/L and 0.52 mU/L for the Chamber 4 and for the Chamber 2, respectively (Figure 4.15). The deviation of the background signal is again really small with the Chamber 4, 2.8×10^3 CPS, compared with the Chamber 2, 7.5×10^3 CPS. Thus the limit of detection value is lower for the Chamber 4 than for the Chamber 2.

This rises up the question about the reliability of the results. The Chamber 4 is sleeker than the Chamber 2 and it should provide a better wash for the reacting surface. This can explain the smaller background deviation, but more experiments are needed to confirm that the deviation is not small just by a change. There are only three parallel samples used in the experiments and thus deviation values may be erroneous. To achieve more reliable results the number of parallel samples should be increased.

5 CONCLUSION

This thesis presented how a finite element method modeling can assist in designing new geometries for microfluidic immunoassays. The model itself was very simplified but it still offered new knowledge about phenomenon occurring inside the reaction chamber. Especially the knowledge on how diffusion is limiting the reactions inside the chamber is now understood much better than before.

FEM-models demonstrated how the mass transfer towards the reaction surface can be increased with a flowing sample. When the chamber size is minimized, the mass transfer can be further increased. The reacting surface outside the measurement area is excess and useless area which is stealing part of an analyte and labels. By minimizing this area, all substances could be used inside the measurement area in order to reach the reaction equilibrium state faster. When the equilibrium is reached, the deviation between parallel samples should also decrease.

Experiments showed that the material of the cartridge has a huge effect on immunoassay performance. Even different polystyrene grades had an effect on signal levels and sensitivities. In most cases, limit of detection values were around 1 mU/L. A challenge in the material was that even though Empera 124N grade was chemically the most suitable for immunoassay cartridges, it was not as good material for injection moulding the chamber geometries as the others. Cartridges made from this material were cracking as they were ejected from an injection moulding device. This can be partially avoided by designing the geometries more carefully and by taking into account the injection moulding process itself.

Other significant result from the experiments was that micro structures increased immunoassay sensitivity nearly 3-fold compared with a smooth surface. The reciprocating flow of the sample in a thin chamber gave 1.4-fold higher sensitivity and the limit of detection was 3.8 times better compared to the stationary incubation in a larger chamber. Combining a micro structured chamber with the moving sample would be an interesting choice for a final cartridge.

Based on the results of the thesis the reaction chamber should have the following characteristics: Small reaction area compared to the volume of the fluid, micro structures on the reacting surface and low a small chamber height. In addition, the reciprocating flow of the sample should be used.

There are several topics to focus on in the future. By focusing on how to prevent unspecific binding it would be possible to decrease background level and its deviation. By doing this the limit of detection should decrease further. The Chamber 3 geometry was modified to the Chamber 4 where washing does not generate bubbles as easy as before. Changing the stationary incubation to a moving sample has shown to be challenging. To achieve a reliable reciprocating movement, it would be possible to use pressure control instead of the syringe pump. Washing protocol should be tested with the Chamber 4 to enhance the washing procedure. At least different flow rates and solution volumes should be tested in order to reach a low background level and standard deviation. For more reliable results, more parallel samples should be used.

Models used in the thesis were really simplified. They did not take into account the unspecific binding of nanoparticles or concentration of the analyte. Adding the effect of analyte concentration would be big challenge to make model more accurate. Nanoparticles are much more complicated to model than single antibodies and thus more knowledge about them is needed. Single antibodies are smaller than nanoparticles and thus they have a higher diffusion coefficient. This would be an option for nanoparticles even though the signal level would decrease. In addition to this the model can be quite easily transformed to use single antibodies as labels. Also a two-phase simulation of reciprocating incubation would be useful in order to more accurately observe how concentration change inside the sample plug. Preliminary tests have shown that a two-phase modeling is much more challenging in comparison with single-phase flows which were used in the thesis.

REFERENCES

[1] K. S. Sashidhar, S. Saha, and G. Ranjith. Western European In Vitro Diagnostics (IVD) Market. Frost & Sullivan, 2012 March.

[2] G. J. Fermann and J. Suyama. Point of care testing in the emergency department. J. Emerg. Med. 22 (2002), 4, pp. 393–404.

[3] P. von Lode. Point-of-care immunotesting: approaching the analytical performance of central laboratory methods. Clin. Biochem. 38 (2005), 7, pp. 591–606.

[4] P. B. Luppa, C. Müller, A. Schlichtiger, and H. Schlebusch. Point-of-care testing (POCT): Current techniques and future perspectives. TrAC Trends Anal. Chem. 30 (2011) 6, pp. 887–898.

[5] C. Chin, V. Linder, and S. Sia. Commercialization of microfluidic point-of-care diagnostic devices. Lab Chip 12 (2012) 12, pp. 2118–2134.

[6] L. Gervais, N. de Rooij, and E. Delamarche. Microfluidic chips for point-of-care immunodiagnostics. Adv. Mater. 23 (2011) 24, pp. H151–176.

[7] A. Ríos, M. Zougagh, and M. Avila. Miniaturization through lab-on-a-chip: utopia or reality for routine laboratories? A review. Anal. Chim. Acta 740 (2012), pp. 1–11.

[8] H. Bruus, Theoretical Microfluidics. New York 2008, Oxford University Press, p. 346.

[9] K. Mohseni. Surface Tension, Capillarity and Contact Angle. In: Encyclopedia of Microfluidics and Nanofluidics. New York 2008, Springer, pp. 1948–1955.

[10] D. Irima. Capillary Force valves. In: Encyclopedia of Microfluidics and Nanofluidics. New York, 2008, Springer, pp. 192–196.

[11] D. Erickson. Electroosmotic Flow (DC). In: Encyclopedia of Microfluidics and Nanofluidics. New York, 2008, Springer, pp. 560–567.

[12] G. L. Morini. Pressure-Driven Single Phase Liguid Flows. In: Encyclopedia of Microfluidics and Nanofluidics. New York, 2008, Springer, pp. 1736–1743.

[13] A. K. Yetisen, M. S. Akram, and C. R. Lowe. Paper-based microfluidic point-of-care diagnostic devices. Lab Chip 13 (2013) 12, pp. 2210–51.

[14] K. Choi, A. H. C. Ng, R. Fobel, and A. R. Wheeler. Digital microfluidics. Annu. Rev. Anal. Chem. 5 (2012), pp. 413–40.

[15] J. Berthier and P. Silberzan. Microfluidics for Biotechnology. 2th edition. Norwood 2010, Artech House, p. 483.

[16] E. L. Cussler, Diffusion: Mass Transfer in Fluid Systems, 3rd edition. Cambridge 2009, Cambridge University Press, p. 631.

[17] C.-Y. Lee, C.-L. Chang, Y.-N. Wang, and L.-M. Fu. Microfluidic mixing: a review. Int. J. Mol. Sci. 12 (2011) 5, pp. 3263–87.

[18] S. Stapleton, R. O'Kennedy, and E. Tully. Production of Antibodies. In: Encyclopedia of Analytical Science. 2nd edition. 2005, Elsevier, pp. 306–316.

[19] C. F. Meares. Bioconjugate Chemistry. In: Encyclopedia of Physical Science and Technology. 2004, Elsevier, pp. 93–98.

[20] Abbot diagnostics. Learning Guide: Immunoassay. [WWW]. Cited 10.9.2013. Available at: http://my.abbottdiagnostics.com/Asse

[21] H. Björkelund, L. Gedda, and K. Andersson. Avoiding false negative results in specificity analysis of protein-protein interactions. J. Mol. Recognit. 24 (2011) 1, pp. 81–89.

[22] T. Näreoja, A. Määttänen, J. Peltonen, P. E. Hänninen, and H. Härmä. Impact of surface defects and denaturation of capture surface proteins on nonspecific binding in immunoassays using antibody-coated polystyrene nanoparticle labels. J. Immunol. Methods 347 (2009) 1–2, pp. 24–30.

[23] C. Selby. Interference in Immunoassay. Ann. Clin. Biochem. 36 (1999), pp. 704–721.

[24] J. Miller. Interference in immunoassays : avoiding erroneous results. Clin. Lab. Int. 28 (2004), pp. 14–17.

[25] L. J. Kricka. Human anti-animal antibody interferences in immunological assays. Clin. Chem. 45 (1999) 7, pp. 942–56.

[26] R. M. Twyman. Immunoassays: Overview. In: Encyclopedia of Analytical Science. 2nd edition. 2005 Elsevier, pp. 299–306.

[27] W. R. Algar, A. J. Tavares, and U. J. Krull. Beyond labels: a review of the application of quantum dots as integrated components of assays, bioprobes, and biosensors utilizing optical transduction. Anal. Chim. Acta. 673 (2010) 1, pp. 1–25.

[28] N. Barié and M. Rapp. Covalent bound sensing layers on surface acoustic wave (SAW) biosensors. Biosens. Bioelectron. 16 (2001) 9–12, pp. 979–987.

[29] R. Raiteri, M. Grattarola, H.-J. Butt, and P. Skládal. Micromechanical cantilever-based biosensors. Sensors Actuators B Chem. 79 (2001), pp. 115–126.

[30] I. Vikholm-Lundin and W. M. Albers. Site-directed immobilisation of antibody fragments for detection of C-reactive protein. Biosens. Bioelectron. 21 (2006) 7, pp. 1141–1148.

[31] E. P. Diamandis. Immunoassays with time-resolved fluorescence spectroscopy: principles and applications. Clin. Biochem. 21 (1988), pp. 139–150.

[32] I. Hemmilä. Luminescent lanthanide chelates—a way to more sensitive diagnostic methods. J. Alloys Compd. 225 (1995), pp. 480–485.

[33] M. A. Kessler. Determination of copper at ng ml^{-1} -levels based on quenching of the europium chelate luminescence. Anal. Chim. Acta. 364 (1998), pp. 125–129.

[34] L. Kokko, T. Lövgren, and T. Soukka. Europium(III)-chelates embedded in nanoparticles are protected from interfering compounds present in assay media. Anal. Chim. Acta. 585 (2007) 1, pp. 17–23.

[35] E. G. Gudgin Dickson, A. Pollak, and E. Diamandis. Ultrasensitive bioanalytical assays using time-resolved fluorescence detection. Pharmacol. Ther. 66 (1995), pp. 207–235.

[36] H. Härmä, T. Soukka, and T. Lövgren. Europium nanoparticles and time-resolved fluorescence for ultrasensitive detection of prostate-specific antigen. Clin. Chem. 47 (2001) 3, pp. 561–568.

[37] T. Soukka, H. Härmä, J. Paukkunen, and T. Lövgren. Utilization of kinetically enhanced monovalent binding affinity by immunoassays based on multivalent nanoparticle-antibody bioconjugates. Anal. Chem. 73 (2001) 10, pp. 2254–60.

[38] O. Aumala. Mittaustekniikan perusteet. 13th edition. Helsinki2006, Otatieto, p. 223.

[39] G. L. Long and J. D. Winefordner. Limit of Detection, A Closer Look at the IUPAC Definition. Anal. Chem. 55 (1983) 7, p. 712A–725A.

[40] A. G. Lalkhen and A. McCluskey. Clinical tests: sensitivity and specificity. Continuing Education in Anaesthesia, Critical Care & Pain 8 (2008) 6, pp. 221–223.

[41] M. Salim, S. L. McArthur, S. Vaidyanathan, and P. C. Wright. Towards proteomics-on-chip: the role of the surface. Mol. Biosyst. 7 (2011) 1, pp. 101–115.

[42] K. Kuwabara, M. Ogino, T. Ando, and A. Miyauchi. Enhancement of fluorescence intensity from an immunoassay chip using high-aspect-ratio nanopillars fabricated by nanoimprinting. Appl. Phys. Lett. 93 (2008) 3, 033904.

[43] P. V Tuttle, A. E. Rundell, and T. J. Webster. Influence of biologically inspired nanometer surface roughness on antigen-antibody interactions for immunoassay-biosensor applications. Int. J. Nanomedicine 1 (2006) 4, pp. 497–505.

[44] H. Labrousse, M. Adib-Conquy, and S. Avrameas. Effect of temperature on the reactivities of polyreactive and monospecific monoclonal IgG antibodies. Res. Immunol. 148 (1997) 4, pp. 267–276.

[45] O. C. Zienkiewicz and R. L. Taylor. The Finite Element Method Fifth edition Volume 1 : The Basis. 2000, Butterworth-Heinemann, p. 689.

[46] O. C. Zienkiewicz and R. L. Taylor. The Finite Element Method Fifth edition Volume 3 : Fluid Dynamics, 2000,Butterworth-Heinemann, p 334.

[47] Comsol Oy, Comsol Multiphysics 4.3b User Guide.

[48] J. Kaakkunen, K. Päiväsaari, and P. Vahimaa. Fabrication of large-area hole arrays using high-efficiency two-grating interference system and femtosecond laser ablation. Appl. Phys. A 103 (2011), pp. 267–270.

[49] J. Ylikotila, L. Välimaa, H. Takalo, and K. Pettersson. Improved surface stability and biotin binding properties of streptavidin coating on polystyrene. Colloids Surf. B. Biointerfaces 70 (2009) 2, pp. 271–7.

[50] A. Mäntymaa, J. Halme, L. Välimaa, and P. Kallio. The effects of laser welding on heterogeneous immunoassay performance in a microfluidic cartridge. Biomicrofluidics 5 (2011) 4, pp. 46504–4650411.